JOURNAL OF PETROLOGY | VOLUME 47 | NUMBER 4 | PAGES 673–703 | 2006 | doi:10.1093/petrology/egi089

Geochemistry of South African On- and Off-craton, Group I and Group II Kimberlites: Petrogenesis and Source Region Evolution

MEGAN BECKER AND ANTON P. LE ROEX*

DEPARTMENT OF GEOLOGICAL SCIENCES, UNIVERSITY OF CAPE TOWN, RONDEBOSCH, 7701, SOUTH AFRICA

RECEIVED MAY 17, 2005; ACCEPTED NOVEMBER 2, 2005; ADVANCE ACCESS PUBLICATION NOVEMBER 29, 2005

Bulk-rock geochemical compositions of hypabyssal kimberlites, emplaced through the Archaean Kaapvaal craton and Proterozoic Namaqua–Natal belt, are used to estimate close-to-primary magma compositions of Group I kimberlites (Mg-number = 0·82–0·87; ~22–28 wt % MgO; ~21–30 wt % SiO_2; ~10–17 wt % CaO; ~0·2–1·7 wt % K_2O) and Group II kimberlites (Mg-number = 0·86–0·89; ~23–29 wt % MgO; ~28–36 wt % SiO_2; 8–13 wt % CaO; ~1·6–4·6 wt % K_2O). Group I kimberlites are distinguished from Group II by their lower Ba/Nb (<12), Th/Nb (<1·1) and La/Nb (<1·1) but higher Ce/Pb (>22) ratios. The distinct rare earth element patterns of the two types of kimberlites indicate a more highly metasomatized source for Group II kimberlites, with more residual clinopyroxene and less residual garnet. The similarity of Sr and Nd isotope ratios and diagnostic trace element ratios (Ce/Pb, Nb/U, La/Nb, Ba/Nb, Th/Nb) of Group I kimberlites to ocean island basalts (OIB), but more refractory Mg-numbers and Ni contents, are consistent with derivation of Group I kimberlites from subcontinental lithospheric mantle (SCLM) that has been enriched by OIB-like melts or fluids. Source enrichment ages and plate reconstructions support a direct association of these melts or fluids with Mesozoic upwelling beneath southern Africa of a mantle plume(s), at present located beneath the southern South Atlantic Ocean. In contrast, the geochemical characteristics of both on- and off-craton Group II kimberlites show strong similarity to calc-alkaline magmas, particularly in their Nb and Ta depletion and Pb enrichment. It is suggested that Group II kimberlites are derived from both Archaean and Proterozoic lithospheric mantle source regions metasomatized by melts or fluids associated with ancient subduction events, unrelated to mantle plume upwelling. The upwelling of mantle plumes beneath southern Africa during the Mesozoic, at the time of Gondwana break-up, may have acted as a heat source for partial melting of the SCLM and the generation of both Group I and Group II kimberlite magmas.

KEY WORDS: *kimberlite; geochemistry; petrogenesis; mantle plumes; South Africa*

INTRODUCTION

Studies of kimberlite magmatism provide a unique opportunity to investigate partial melting processes in the deeper parts of the Earth's upper mantle. Their unique ultramafic, potassic and volatile-rich character, with enrichment in both compatible and incompatible trace elements, suggests derivation from mantle source regions with a complex evolutionary history. Although there have been numerous studies focused on characterizing the major element geochemistry (e.g. Clement, 1982; Shee, 1985), trace element geochemistry (e.g. Wedepohl & Muramatsu, 1975; Smith *et al.*, 1985*b*) or isotope geochemistry (e.g. Smith, 1983; Fraser *et al.*, 1985–1986; Nowell *et al.*, 2004), only relatively recently has trace element geochemistry been used to constrain petrogenetic processes and the evolution of kimberlite source regions (e.g. Fraser & Hawkesworth, 1992; Tainton & McKenzie, 1994; Beard *et al.*, 1998; le Roex *et al.*, 2003; Chalapathi Rao *et al.*, 2004; Coe, 2004; Harris *et al.*, 2004).

Semi-quantitative genetic models argue for derivation of kimberlite by very low degrees of partial melting of metasomatically enriched, previously melt-depleted, garnet peridotite facies lithospheric mantle (Tainton & McKenzie, 1994; le Roex *et al.*, 2003; Harris *et al.*, 2004). Such models are consistent with experimental studies suggesting carbonated garnet peridotite source regions (e.g. Dalton & Presnall, 1998*a*; Ulmer & Sweeney, 2002). More exotic source regions such as garnetite (Edgar & Charbonneau, 1993) and clinopyroxene and mica-rich veins (Foley, 1992*b*) have, however, also been suggested.

*Corresponding author. E-mail: aleroex@geology.uct.ac.za

Two broad varieties of southern African kimberlites are recognized, and have been classified variously as 'basaltic' and 'micaceous' (on petrographic grounds; Wagner, 1914), 'Group I' and 'Group II' (on isotopic grounds; Smith, 1983) or 'kimberlite' and 'orangeite' (Mitchell, 1995). Group I kimberlites are defined as being slightly less radiogenic in terms of their Sr isotope and more radiogenic in terms of their Nd isotope compositions than present-day Bulk Earth, and in this regard show similarity to ocean island basalts (OIB). Smith (1983) associated such kimberlites with a sub-lithospheric mantle source. Group II kimberlites, which tend to be more micaceous, have highly radiogenic Sr isotope compositions relative to Bulk Earth and have been associated with direct derivation from the subcontinental lithospheric mantle (SCLM; Smith, 1983; Fraser *et al.*, 1985–1986; Tainton & McKenzie, 1994; Coe, 2004). The interpretation of the results of Hf isotope studies are variable; Nowell *et al.* (2004) have proposed that both Group I and Group II kimberlites have sub-lithospheric sources, whereas Griffin *et al.* (2000) and Choukroun *et al.* (2005) preferred a model with contributions from both asthenospheric and sub-lithospheric mantle sources. Similarly, le Roex *et al.* (2003) have argued for a two-stage model for the generation of Group I kimberlites, involving both sub-lithospheric and lithospheric mantle source components.

The origin of both Group I and Group II Mesozoic kimberlites within southern Africa, from both on-craton and off-craton settings, is investigated in this study. This is done by combining major and trace element and isotope and subsequently developing semi-quantitative genetic models. These models are aimed at identifying petrogenetic processes and source region compositions that can account for the observed similarities and differences. Possible causes of kimberlite source region enrichment (metasomatism), and the origin of metasomatic melts or fluids, are also explored.

To achieve these objectives, close-to-primary magma compositions for the individual kimberlites analysed in this study are determined, after taking into account the effects of various secondary processes and fractional crystallization. Semi-quantitative modelling of kimberlite genesis and source geochemistry is used to evaluate mantle source region characteristics and evolutionary processes, as a basis for the development of an integrated model describing the petrogenesis of South African Group I and Group II Mesozoic kimberlites.

GEOLOGICAL SETTING AND SAMPLING

Kimberlites in southern Africa have been emplaced either through the Archaean Kaapvaal craton (de Wit *et al.*, 1992; 'on-craton kimberlites') or through the surrounding Namaqua–Natal Mesoproterozoic metamorphic belt (off-craton kimberlites). Most of the 23 Group I and Group II kimberlites that form the basis of this study crop out within the shales, mudstones and sandstones of the Phanerozoic Karoo Supergroup, and range in age from ~74 Ma to ~150 Ma (Davis, 1977; Smith *et al.*, 1985*a*, 1994); the Group II kimberlites are predominantly older than the Group I kimberlites.

On-craton kimberlites analysed in this study (Fig. 1; Table 1) are the Group I kimberlite occurrences at Koffiefontein, Jagersfontein and Monastery, and the Bellsbank, Newlands, New Elands and Finsch Group II kimberlites. Off-craton kimberlites comprise the Abbotsford East and Zeekoegat Group I kimberlites from East Griqualand (Nixon *et al.*, 1983), as well as Group I and Group II kimberlites located within the vicinity of Victoria West, Prieska and Hanover (Robey, 1981; Skinner *et al.*, 1992). Some of the kimberlites located near Prieska and Hanover are inferred to have been emplaced within Archaean crystalline basement (e.g. Goedehoop, Andriesfontein kimberlites) according to their relationship to the Brakbos fault, the generally accepted border between Proterozoic and Archaean Provinces (Pretorious, 1974; Cornell *et al.*, 1986; Schmitz *et al.*, 2004). In this study these kimberlites are considered to be on-craton.

Sampling was focused on hypabyssal kimberlite to avoid the excessive alteration and contamination present in most diatreme-facies kimberlite; material was selected to avoid obvious alteration, weathering and crustal contaminants. Where possible, multiple samples were collected from individual kimberlite bodies; the final sample suite includes material recovered from field outcrop, underground mine workings, collections housed at the University of Cape Town and collections provided by the De Beers Geoscience Centre.

ANALYTICAL TECHNIQUES

All samples were prepared for geochemical analysis at the University of Cape Town (UCT). Weathered surfaces were removed using a hydraulic splitter, after which samples were split and passed through a jaw crusher. The jaw crush chips were individually hand picked, with careful attention being paid to selecting kimberlite fragments free from weathering, crustal and mantle xenoliths, megacrysts and calcite veining. The clean samples were then powdered using a Sieb swing mill and carbon steel vessel. A subset of kimberlites was received from the De Beers Geoscience Centre as powders (K16/6; K51/2; K19/15; K5/P2; K6/11; K2/2 and K2/13) and, therefore, could not be prepared as desired.

Major element and Ni and Cr concentrations were determined by X-ray fluorescence (XRF) on a Philips

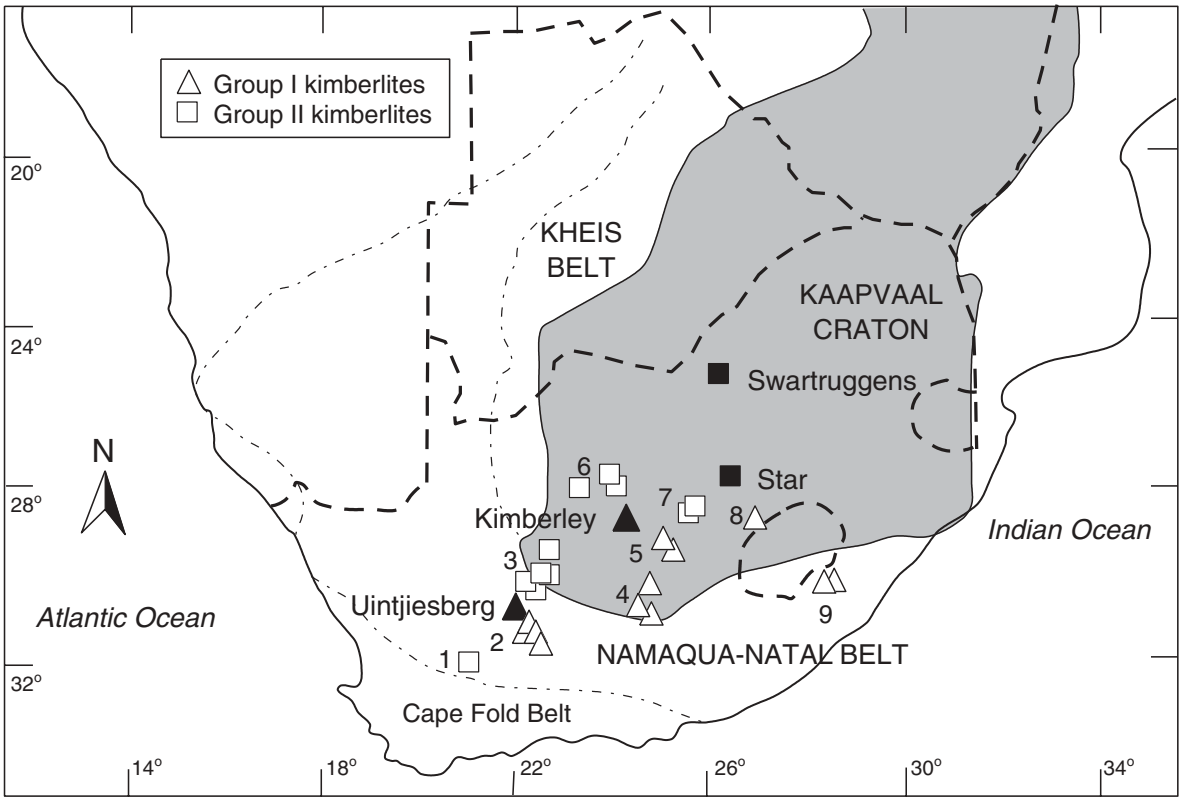

Fig. 1. Location of on- and off-craton Group I and Group II kimberlites analysed in this study relative to the Kaapvaal craton (shaded in grey). Light dot–dash boundary represents the Namaqua–Natal mobile belt. Figure adapted from Carlson *et al.* (2000). Filled symbols indicate locations of the Kimberley Group I kimberlites, the off-craton Uintjiesberg Group I kimberlite and the Star and Swartruggens Group II kimberlites. Numbers represent clusters of kimberlites; for individual kimberlites localities and coordinates are given in Table 1.

X'Unique wavelength-dispersive spectrometer using a low dilution fusion technique (Willis, 1999). Selected trace elements (Co, V, Cu, Nb and Zr) were determined by XRF on 6 g powder briquettes with accuracy and precision values for XRF analyses similar to those reported by le Roex *et al.* (1981). A more comprehensive set of trace elements including the rare earth elements (REE) was analysed by solution inductively coupled plasma mass spectrometry (ICP-MS) on a Perkin–Elmer ELAN 6000 system. A detailed description of the sample preparation techniques and analyses of procedural blanks and standards has been given by le Roex *et al.* (2001, 2003). The relative standard deviation for most elements was generally better than 3%. Zr and Nb data by XRF and ICP-MS generally show good agreement, suggesting that incomplete dissolution of Fe–Ti-oxides or zircon was not a significant problem. CO_2 was determined using a Karbonat Bombe according to the method described by Birch (1981), with relative precision between 2 and 5%.

Representative samples were prepared for Sr and Nd isotope analysis by thermal ionization mass spectrometry (TIMS) on a VG Sector seven-collector system run in multi-dynamic mode, using standard ion exchange techniques as described by Hart (1977) and Zindler (1980). $^{87}Sr/^{86}Sr$ isotope ratios were normalized against a $^{86}Sr/^{88}Sr$ ratio of 0·1194 and $^{143}Nd/^{144}Nd$ against a $^{146}Nd/^{144}Nd$ ratio of 0·7219. International standards NBS 987 and La Jolla yielded $^{87}Sr/^{86}Sr$ and $^{143}Nd/^{144}Nd$ ratios of $0{\cdot}710260 \pm 17$ (2σ; $n = 3$) and $0{\cdot}511829 \pm 10$ (2σ; $n = 1$), respectively.

PETROGRAPHY

The analysed kimberlites can be divided according to texture into macrocrystic and aphanitic varieties (Clement & Skinner, 1979; Clement *et al.*, 1984). The non-genetic textural term 'macrocrystic' is used to indicate the presence of predominantly large, anhedral, olivine crystals (>2 mm) that may have been derived from disaggregated mantle xenoliths (Clement *et al.*, 1984; le Roex *et al.*, 2003). All samples with >10 vol. % macrocrysts are classified as macrocrystic. More euhedral olivine and phlogopite crystals, >1 mm in size, are referred to as phenocrysts and if <1 mm, as microphenocrysts. Mineral abundances are summarized for representative kimberlite samples in Table 1.

Table 1: Summary table of kimberlite coordinates and locations as illustrated in Fig. 1

Kimberlite	Sample	Fig. 1 ref.	Latitude (°S)	Longitude (°E)	Macrocrysts (%)			Phenos and microphenos	Groundmass and accessory minerals	Classification
					Ol	Phlog	Other			
Group I kimberlites: on-craton										
Andriesfontein	ADF 1	4	30°57′	24°36′	10	5		ol	calc, serp, phlog, op-ox, pv, ap, zeol	Serpentine calcite kimberlite
Goedehoop	JJG 4282	4	30°50′	24°25′	10	5		ol	calc, serp, op-ox, pv, ap	Serpentine calcite kimberlite
Jagersfontein	JJG 2151	5	29°46′	25°27′	25	5	op-ox	ol	calc, serp, phlog, op-ox, pv, ap	Serpentine calcite kimberlite
Koffiefontein	KK 3	5	29°25′	25°00′	15			ol	calc, serp, phlog, op-ox, pv, ap	Serpentine calcite kimberlite
Lekkerfontein	LKF 1	4	30°20′	24°38′	1	1	op-ox	ol, phlog	calc, serp, phlog, op-ox, pv	Calcite kimberlite
Monastery	ROM 312	8	28°49′	27°25′	10	2	op-ox	ol	calc, serp, phlog, op-ox, pv	Phlogopite calcite kimberlite
Group I kimberlites: off-craton										
Abbotsford East	JJG 3118	9	30°27′	28°50′	10			ol	calc, serp, phlog, op-ox, pv	Calcite kimberlite
Gansfontein	GNF 2	2	31°46′	22°33′	12	3	op-ox	ol	calc, serp, op-ox, pv, zeol	Op-ox-rich calc. serp kimberlite
Hebron	HEB 1A	2	31°17′	22°34′	7	13	op-ox	ol	calc, serp, op-ox, pv, ap	Serpentine calcite kimberlite
Klipgatsfontein	JJG 4323	2	31°19′	22°37′	5	17	op-ox	ol	calc, serp, op-ox, pv	Serpentine calcite kimberlite
Pampoenpoort	K16/6W	2	31°07′	22°43′	—	—				Op-ox rich mont. kimb. (Clark, 1994)
Zeekoegat	JJG 1906	9	30°27′	28°50′	15			ol	calc, serp, phlog, op-ox, pv	Calcite kimberlite
Group II kimberlites: on-craton										
Bellsbank	JJG 4676	6	28°05′	24°02′	25	5		ol	calc, serp, phlog, op-ox, pv, ap	Calcite phlogopite kimberlite
Finsch	CRC 7	6	28°21′	23°27′	19·5	0·5		ol, phlog	calc, phlog, op-ox, pv	Phlogopite kimberlite
Jonkerwater	K51/2W	3	30°10′	22°38′	—	—				Phlogopite kimberlite (Clark, 1994)
Middlewater	K19/15W	3	30°10′	22°43′	—	—				Carb. phlog. kimb. (Clark, 1994)
New Elands	NE K6	7	28°31′	25°29′	10			ol	calc, serp, phlog, op-ox, pv, ap	Calcite phlogopite kimberlite
Newlands	JJG 24	6	28°20′	24°02′	19	5	op-ox, gnt	ol	calc, serp, phlog, op-ox, pv, ap	Phlogopite kimberlite
Roberts Victor	RVK 2	7	28°30′	25°33′	25	5		ol, phlog	calc, serp, phlog, op-ox, pv, ap	Calcite phlogopite kimberlite
Sanddrift	K5/P2	3	29°30′	22°56′	—	—				Phlogopite kimberlite (Clark, 1994)
Group II kimberlites: off-craton										
Brandewynskuil	K6/11	3	30°37′	22°41′	15	5		ol, phlog	serp, phlog, diop, op-ox, pv	Serpentine phlogopite kimberlite
Eendekuil	K2/2	1	32°15′	20°59′	5	20		ol, phlog	calc, phlog, op-ox, pv	Phlogopite calcite kimberlite
Markt	MRK 3	3	30°15′	22°21′	15	5		ol	calc, serp, phlog, op-ox, pv, ap	Calcite phlogopite kimberlite

Macrocryst, phenocryst and groundmass phases in representative Group I and Group II kimberlite samples are given. Volume percentages of macrocrysts, defined by visual estimation, are also given for reference. Modal data are missing from samples provided as powders by De Beers Geoscience Centre. ol, olivine; phlog, phlogopite; gnt, garnet; calc, calcite; serp, serpentine; diop, diopside; op-ox, opaque oxide (includes ilm); pv, perovskite; ap, apatite, zeol, zeolite; mont, monticellite; carb, carbonate.

JOURNAL OF PETROLOGY | VOLUME 47 | NUMBER 4 | APRIL 2006

Both on- and off-craton Group I kimberlites are mineralogically classified as serpentine calcite or calcite kimberlites (Table 1; using the classification scheme proposed by Clement & Skinner, 1979); most are sparsely macrocrystic to macrocrystic in texture, except for the aphanitic Lekkerfontein kimberlite. The subhedral to anhedral olivine macrocrysts, which may be up to 10 mm in size, are variably serpentinized and sometimes chloritized, and are the most abundant macrocryst phase (10–33 vol. %), whereas phlogopite (<10 vol. %) and ilmenite (<5 vol. %) are less abundant. Phlogopite macrocrysts tend to be corroded and show undulose extinction or kink banding, as well as, in some samples (Goedehoop, Klipgatsfontein, Hebron kimberlites), the development of calcite stringers along cleavage planes. Rare ilmenite macrocrysts, characterized by groundmass perovskite aggregations along their rims, are possibly correlated with the kimberlite 'megacryst suite', including zircon, known to occur in these kimberlites (e.g. Monastery, Lekkerfontein and Gansfontein kimberlites; Boyd & Nixon, 1975; Monastery, Lekkerfontein and Gansfontein kimberlites; Robey, 1981).

Euhedral to subhedral olivine phenocrysts and microphenocrysts are present in all the analysed Group I kimberlites, varying in abundance between 10 and 30 vol. %. In contrast, phlogopite phenocrysts occur in only two of the samples (JJG 4295, LKF 1). Fine-grained calcite and serpentine are the predominant groundmass phases, forming either a uniform or segregationary texture (Clement & Skinner, 1979), with some of the segregations showing very well-developed rhombohedral calcite crystals up to 500 μm in size. Calcite segregations can reach up to a few millimetres in size. Scattered, stubby-shaped groundmass phlogopite crystals occur in most kimberlites except for Goedehoop, Hebron and Kligatsfontein, whereas equant groundmass opaque oxide and lesser amounts of perovskite crystals (~100 μm) are ubiquitous. In comparison with other on-craton kimberlites (e.g. Kimberley kimberlites, Clement, 1982), the off-craton kimberlites in this study appear not to be characterized by the presence of groundmass monticellite. However, given that primary monticellite is prone to alteration, forming secondary serpentine and calcite (Clement, 1982), its paucity may reflect the more altered nature of the off-craton kimberlites.

Both on- and off-craton Group II kimberlites are classified as phlogopite kimberlites or calcite phlogopite/phlogopite calcite kimberlites and vary in texture between sparsely macrocrystic and macrocrystic (up to 45 vol. % macrocrysts). Anhedral olivine macrocrysts, up to 15 mm in size, are variably altered, by serpentinization along fractures, calcitization in patches or chloritization along their rims. Strained phlogopite macrocrysts (up to 20 vol. %) show strong pleochroism and are rimmed by tetraferriphlogopite or chlorite (e.g. Newlands kimberlite). In the off-craton Eendekuil kimberlite, the phlogopite macrocrysts show slight flow alignment. Garnet macrocrysts, rimmed by kelyphite or chlorite, were also identified in a few of the kimberlite samples (Newlands: JJG 24, KN 2; Markt: MRK 3).

Olivine phenocrysts are ubiquitous in all of the analysed Group II kimberlites and may constitute up to 35 vol. % of the rock. Tabular phlogopite phenocrysts, rimmed by tetraferriphlogopite, are also common, whereas subdhedral diopside phenocrysts were identified only in Eendekuil kimberlite sample EKL 1. Short, stubby, interlocking phlogopite crystals, rimmed by tetraferriphlogopite, form the dominant (15–40 vol. %) groundmass phase in most of the analysed Group II kimberlites; these vary in size from being very fine-grained (50–100 μm) to fine-grained (100–500 μm). Groundmass calcite is the next most common matrix phase (up to 30 vol. %) and is generally interstitial, although it may sometimes form calcite segregations up to 4 mm in size. Although matrix serpentine was recognized in a few kimberlite samples, it is likely that some is secondary in origin (e.g. Brandewynskuil kimberlite). Similarly, the chloritization of groundmass phlogopite in some kimberlites (Bellsbank and Newlands) and pervasive carbonatization in others (Roberts Victor, RVK 1) is inferred to be an alteration feature. Accessory opaque oxides and perovskite crystals are very fine-grained (20–50 μm) and relatively sparse; perovskite crystals may be poikilitically enclosed in phlogopite microphenocrysts (e.g. New Elands kimberlite). Trace amounts of apatite needles, 50–500 μm in size, have also been recognized in the Bellsbank, New Elands, Newlands, Roberts Victor and Markt kimberlites. No significant petrographic differences are recognized between on- and off-craton Group II kimberlites.

GEOCHEMISTRY

The major and trace element compositions of selected on- and off-craton kimberlites are reported in Table 2, with Nd–Sr isotope compositions in Table 3. The complete kimberlite dataset used in this study is available online (Electronic Appendix 1; http://www.petrology.oupjournals.org). The data are supplemented with analyses from the on-craton Group I Kimberley kimberlites (le Roex *et al.*, 2003), Swartruggens and Star Group II kimberlites (Coe, 2004) shown as fields, and with analyses from the off-craton Group I Uintjiesberg kimberlite (Harris *et al.*, 2004), shown as data points in Figs 2–6.

On- and off-craton Group I kimberlites

SiO_2 and MgO concentrations of Group I kimberlites show broad positive correlations (Fig. 2a) with SiO_2

Table 2: Bulk-rock geochemical analyses of on- and off-craton Group I and Group II kimberlites, analysed by XRF and ICP-MS

	Group I kimberlites: on-craton						Group I kimberlites: off-craton					
Kimberlite:	Andriesfontein	Goedehoop	Jagersfontein	Koffiefontein	Lekkerfontein	Monastery	Abbotsford East	Gansfontein	Hebron	Klipgatsfontein	Pampoenpoort	Zeekoegat
Sample:	ADF 1	JJG 4282	JJG 2151	KK 3	LKF 1	ROM 312	JJG 3118	GNF 2	HEB 1A	JJG 4323	K16/6W	JJG 1906
% Macro.:	15	15	30	15	2	12	10	15	25	27	—	15
SiO_2	26·78	26·10	31·91	32·10	22·47	26·92	23·45	27·78	26·35	24·96	30·23	24·80
TiO_2	1·75	3·25	1·04	2·30	4·53	4·21	2·63	4·92	3·32	2·95	1·95	2·54
Al_2O_3	2·69	2·54	2·24	3·07	4·43	2·77	3·19	4·25	2·78	3·11	2·34	3·43
Fe_2O_3	9·99	13·15	8·54	10·04	13·33	13·46	11·39	16·67	11·07	11·93	9·91	11·48
MnO	0·17	0·23	0·17	0·16	0·22	0·19	0·20	0·21	0·16	0·19	0·16	0·20
MgO	25·63	25·82	33·25	26·28	18·63	28·11	23·29	24·98	23·18	24·33	30·67	25·31
CaO	12·67	12·27	6·97	9·68	15·37	9·34	16·70	8·32	13·84	14·23	8·81	14·31
Na_2O	0·31	0·27	0·38	0·11	0·25	0·25	0·17	0·39	0·14	0·08	0·41	0·03
K_2O	0·99	0·23	0·82	1·43	1·63	1·01	0·20	1·86	0·50	0·39	1·08	0·26
P_2O_5	4·18	2·11	2·78	0·97	1·49	0·89	0·79	1·17	0·99	1·71	0·81	0·33
SO_3	0·03	0·10	0·04	0·47	n.d.	0·02	0·41	0·15	n.d.	0·17	0·04	0·79
NiO	0·16	0·11	0·15	0·14	0·05	0·12	0·08	0·04	0·09	0·08	0·16	0·10
Cr_2O_3	0·18	0·17	0·27	0·22	0·16	0·15	0·13	0·07	0·13	0·12	0·23	0·15
H_2O^-	0·82	0·49	0·45	0·62	1·42	1·05	0·52	0·44	1·18	0·98	0·41	0·21
LOI	13·39	12·83	10·59	11·87	15·55	10·72	16·71	8·02	16·20	14·65	12·37	15·32
Total	99·74	99·67	99·60	99·46	99·53	99·19	99·84	99·29	99·93	99·88	99·58	99·24
H_2O^+	7·89	6·53	—	6·92	5·92	6·27	6·51	6·42	6·11	3·85	6·15	4·82
CO_2	5·50	6·30	—	4·96	9·63	4·45	10·19	1·60	10·09	10·79	6·22	10·49
Cl	1·12	1·1	1·01	1·2	1·34	1·03	1·1	1·13	1·2	1·1	1·04	1·1
Mg-no.	0·85	0·82	0·89	0·86	0·76	0·81	0·82	0·77	0·83	0·82	0·87	0·83
XRF												
Zr	435	453	392	253	2078	643	353	1751	274	354	267	377
Nb	192	297	417	157	336	243	128	318	136	160	140	110
Co	74·3	86·6	81·8	102	54·9	97·8	96·7	123	95·9	85·9	101	90·0
Cr	1228	1191	1819	1532	1064	1034	889	451	865	808	1545	993
Ni	1242	844	1198	1079	421	905	644	352	682	663	1240	762
V	127	158	57·7	139	347	174	217	185	220	169	131	150
Cu	249	60·2	35·8	74·3	160	102	154	115	87·4	87·2	40·8	137

	Group I kimberlites: on-craton						Group I kimberlites: off-craton					
Kimberlite:	Andriesfontein	Goedehoop	Jagersfontein	Koffiefontein	Lekkerfontein	Monastery	Abbotsford East	Gansfontein	Hebron	Klipgatsfontein	Pampoenpoort	Zeekoegat
Sample:	ADF 1	JJG 4282	JJG 2151	KK 3	LKF 1	ROM 312	JJG 3118	GNF 2	HEB 1A	JJG 4323	K16/6W	JJG 1906
% Macro.:	15	15	30	15	2	12	10	15	25	27	—	15
ICP-MS												
Sc	13·9	23·4	14·8	12·2	19·4	14·8	18·0	19·5	14·9	18·3	10·3	16·8
Rb	64·2	16·9	37·2	82·3	112	93·9	10·2	80·0	49·1	28·2	51·8	8·93
Sr	2368	1164	1131	816	1810	1071	998	1154	733	1010	821	447
Y	16·8	35·5	17·8	13·8	33·6	19·8	17·5	23·4	14·7	19·3	11·7	16·9
Zr	379	436	375	247	1935	548	341	1706	260	341	251	369
Nb	172	316	390	166	298	216	138	337	142	167	130	117
Ba	1079	1572	2276	707	1330	1170	281	1204	920	721	929	168
La	109	238	292	131	253	140	80·9	196	80·4	121	96·1	66·7
Ce	207	481	579	259	494	275	163	383	158	238	189	143
Pr	21·8	51·1	60·0	26·7	50·6	29·7	17·8	40·2	17·0	25·8	20·3	16·0
Nd	83·1	201	218	98·0	190	110	69·7	156	68·8	102	75·0	63·6
Sm	12·2	30·0	26·4	13·0	26·3	16·2	10·9	22·7	10·9	15·9	10·5	10·0
Eu	3·39	7·81	6·40	3·28	7·03	4·33	2·79	5·65	3·00	4·08	2·77	2·53
Gd	9·05	21·0	16·2	8·49	18·6	11·7	8·10	15·0	8·02	11·2	7·27	7·54
Tb	1·03	2·25	1·63	0·93	2·11	1·34	0·94	1·59	0·89	1·22	0·78	0·88
Dy	4·41	9·93	5·69	3·88	9·03	5·53	4·54	6·81	4·02	5·39	3·20	4·357
Ho	0·67	1·44	0·77	0·58	1·33	0·83	0·70	0·98	0·60	0·81	0·47	0·69
Er	1·42	3·21	1·51	1·27	2·89	1·76	1·65	2·17	1·41	1·87	1·06	1·64
Tm	0·16	0·34	0·16	0·15	0·33	0·18	0·19	0·22	0·15	0·20	0·11	0·19
Yb	0·85	1·75	0·79	0·79	1·83	1·01	1·07	1·36	0·85	1·07	0·62	1·07
Lu	0·10	0·21	0·11	0·10	0·21	0·12	0·13	0·14	0·10	0·13	0·08	0·13
Hf	6·96	8·30	5·85	5·12	41·3	12·0	7·24	38·8	6·28	7·33	4·83	8·48
Ta	6·15	14·1	16·2	8·55	14·8	11·7	8·20	20·5	9·57	9·57	5·86	7·73
Pb	7·70	11·8	13·7	9·00	15·2	6·86	4·83	11·1	5·10	8·01	5·48	9·98
Th	14·1	31·8	48·0	15·5	39·0	17·7	10·6	26·1	10·1	16·7	11·7	9·03
U	4·03	7·26	10·8	3·50	10·3	4·33	2·48	6·48	2·54	3·86	3·15	2·06

Table 2: *continued*

	Group II kimberlites: on-craton								Group II kimberlites: off-craton		
Kimberlite:	Bellsbank	Finsch	Jonkerwater	New Elands	Newlands	Roberts Victor	Middelwater	Sanddrift	Brandewynskuil	Eendekuil	Markt
Sample:	JJG 4676	CRC 7	K51/2W	NE K6	JJG 24	RVK 2	K19/15W	K5/P2	K6/11*	K2/2	MRK 3
% Macro.:	30	20	—	10	25	30	—	—	20	25	20
SiO_2	33·42	39·06	31·82	35·97	33·59	34·21	38·54	35·97	41·01	31·81	31·53
TiO_2	0·87	0·81	0·84	1·43	0·69	3·62	0·91	0·69	1·24	2·55	0·86
Al_2O_3	1·97	3·36	3·03	4·31	2·08	0·96	3·12	2·82	6·43	5·42	2·74
Fe_2O_3	7·80	8·84	7·43	9·02	7·85	7·60	8·06	7·13	7·67	9·69	7·63
MnO	0·15	0·15	0·14	0·23	0·13	0·13	0·16	0·16	0·11	0·18	0·16
MgO	31·76	30·6	27·70	23·86	32·74	29·71	26·77	28·89	20·40	10·67	27·14
CaO	8·07	6·77	9·49	8·08	6·35	7·17	4·84	5·09	6·15	18·26	10·73
Na_2O	0·12	0·61	0·34	0·23	<0·01	0·18	0·37	0·48	0·36	0·07	0·03
K_2O	1·89	2·82	2·06	4·56	1·26	2·23	3·53	2·55	3·17	4·15	2·32
P_2O_5	2·12	0·62	1·90	1·10	1·78	1·56	0·66	0·03	1·06	0·97	1·69
SO_3	0·10	0·13	0·09	0·03	0·24	0·26	0·05	0·06	—	0·61	0·02
NiO	0·17	0·18	0·14	0·12	0·20	0·26	0·18	0·19	—	0·04	0·11
Cr_2O_3	0·25	0·31	0·25	0·21	0·28	0·14	0·26	0·28	—	0·08	0·28
H_2O^-	0·44	0·56	0·65	1·57	0·43	0·62	1·57	1·63	3·97	0·56	0·32
LOI	10·26	4·58	13·18	9·21	11·45	11·01	10·45	13·76	8·42	14·41	13·55
Total	99·39	99·03	99·06	99·92	99·06	99·67	99·47	99·72	99·99	99·46	99·11
H_2O^+	5·16	3·10	5·45	—	7·15	7·26	7·00	7·00	8·22	0·02	7·16
CO_2	5·10	1·48	7·73	—	4·30	3·75	3·45	6·76	0·20	14·39	6·40
Cl	1·0	1·2	1·2	1·2	1·0	1·0	1·4	1·2	1·8	2·0	1·1
Mg-no.	0·80	0·89	0·89	0·86	0·90	0·89	0·88	0·90	0·86	0·71	0·89
XRF											
Zr	317	178	407	468	224	552	154	137	297	168	350
Nb	226	49·0	148	106	163	126	56·3	50·1	67·0	142	105
Co	80·5	84·2	84·5	72·0	83·9	71·5	92·4	91·6	77·0	77·2	82·9
Cr	1740	2121	1730	1428	2248	1605	1762	1892	1412	558	1936
Ni	1297	1414	1125	875	1380	1190	1437	1489	972	287	885
V	71·9	86·1	185	103	54·0	42·1	116	39·1	131	241	56·8
Cu	56·9	41·8	23·5	54·0	80·0	19·0	24·6	2·62	28·0	64·4	42·3

	Group II kimberlites: on-craton								Group II kimberlites: off-craton		
Kimberlite:	Bellsbank	Finsch	Jonker-water	New Elands	Newlands	Roberts Victor	Middelwater	Sanddrift	Brandewynskuil	Eendekuil	Markt
Sample:	JJG 4676	CRC 7	K51/2W	NE K6	JJG 24	RVK 2	K19/15W	K5/P2	K6/11*	K2/2	MRK 3
% Macro.:	30	20	—	10	25	30	—	—	20	25	20
ICP-MS											
Sc	22·5	19·2	23·4	16·3	15·1	23·4	9·1	12·7	17·3	14·2	29·5
Rb	120	138	69·4	165	72·9	69·3	138	86·0	103	187	80·8
Sr	1947	845	1874	1358	1000	1529	780	587	1453	1438	1677
Y	15·2	7·99	21·9	19·8	9·69	26·4	9·04	6·00	16·5	18·6	15·6
Zr	276	178	366	317	199	521	144	128	299	147	343
Nb	222	51·2	132	102	158	127	48·9	45·9	72·4	133	107
Ba	2617	1479	5446	2414	3883	3615	1724	1733	1786	1692	3569
La	390	55·5	241	211	231	370	67·8	73·3	135	177	189
Ce	708	115	493	410	424	744	137	161	273	342	391
Pr	69·1	13·4	53·2	41·9	40·6	76·3	15·1	17·9	28·6	34·4	41·9
Nd	224	51·2	191	147	129	262	55·5	64·4	105	126	157
Sm	21·5	6·64	23·1	16·9	13·0	26·6	7·34	7·30	12·6	15·5	19·3
Eu	4·57	1·59	5·70	3·94	2·78	5·92	1·91	1·73	2·76	3·56	4·57
Gd	11·5	3·87	13·8	10·2	6·60	14·2	4·79	4·07	7·31	9·28	10·6
Tb	1·26	0·44	1·51	1·15	0·72	1·55	0·55	0·45	0·79	1·00	1·11
Dy	4·37	1·95	5·74	4·89	2·70	6·80	2·31	1·63	3·83	4·72	4·35
Ho	0·65	0·32	0·90	0·78	0·40	1·05	0·36	0·24	0·62	0·71	0·63
Er	1·45	0·76	1·98	1·77	0·92	2·43	0·82	0·55	1·48	1·55	1·49
Tm	0·17	0·10	0·24	0·21	0·11	0·28	0·10	0·07	0·18	0·17	0·16
Yb	0·93	0·60	1·34	1·18	0·60	1·60	0·56	0·42	1·17	0·93	0·90
Lu	0·12	0·08	0·18	0·15	0·08	0·20	0·07	0·05	0·15	0·10	0·12
Hf	7·21	3·91	7·86	8·71	4·25	11·5	3·12	3·24	6·60	3·73	6·52
Ta	11·8	3·33	3·91	4·58	7·40	5·81	0·89	1·69	3·96	7·27	5·33
Pb	35·0	22·0	34·2	35·7	26·6	25·4	16·6	2·31	10·4	25·3	24·0
Th	56·7	6·69	28·8	20·7	35·0	50·2	8·07	7·38	16·4	25·3	22·7
U	6·95	2·35	6·23	4·05	4·14	4·34	2·28	1·58	2·26	2·27	5·76

*Major and XRF trace element analyses from Clark (1994).
All Fe is reported as Fe_2O_3, Mg-number (Mg-number) is atomic Mg/(Mg + Fe^{2+}), calculated using an Fe_2O_3/FeO ratio of 0·15. H_2O^+ is defined as the difference between the loss on ignition (LOI) and CO_2 concentrations. The contamination index (CI) defined by Clement (1982) is also given for reference. —, not determined.

Table 3: Measured Sr and Nd isotope ratios and calculated parent/daughter ratios for on- and off-craton, Group I and Group II kimberlites

Kimberlite	Sample	Rb	Sr	$^{87}Rb/^{86}Sr$	$^{87}Sr/^{86}Sr_{(M)}$	2σ	Age	$^{87}Sr/^{86}Sr_{(i)}$	Sm	Nd	$^{147}Sm/^{144}Nd$	$^{143}Nd/^{144}Nd_{(M)}$	2σ	$^{143}Nd/^{144}Nd_{(i)}$
Group I kimberlites: on-craton														
Andriesfontein kimberlite	ADF 1	64·2	2368	0·0785	0·703727	17	74*	0·703644	12·18	83·13	0·0886	0·512678	9	0·512635
Big Hole–kimberlite pipe	COL6	96·3	1167	0·2387	0·704787	18	84	0·704502	12·33	82·34	0·0905	0·512655	10	0·512605
Big Hole–kimberlite pipe	COL9	58	1011	0·1669	0·707675	20	84	0·707475	11·06	74·45	0·0898	0·512636	12	0·512587
Bultfontein kimberlite	K8/17	31·6	1443	0·0633	0·704060	17	84	0·703985	34·17	228·50	0·0904	0·512661	10	0·512611
Bultfontein kimberlite	K8/115	14·1	1387	0·0294	0·705405	18	84	0·705370	12·35	86·96	0·0859	0·512624	9	0·512577
De Beers kimberlite	C16	70·7	1215	0·1684	0·705035	18	84	0·704834	14·25	98·01	0·0879	0·512590	15	0·512542
De Beers kimberlite	K3/608	14·1	1851	0·0220	0·704623	17	84	0·704597	24·80	178·39	0·0840	0·512618	8	0·512572
Dutoitspan kimberlite	K6/55	77·0	1666	0·1338	0·705063	18	84	0·704903	21·56	157·26	0·0829	0·512636	9	0·512590
Goedehoop kimberlite	JAR 30012	16·6	1072	0·0448	0·703633	18	74*	0·703586	27·1	181	0·0905	0·512732	8	0·512688
Goedehoop kimberlite	JJG 4282	16·9	1164	0·0420	0·703731	15	74*	0·703687	30·0	201	0·0902	0·512738	9	0·512695
Jagersfontein kimberlite	JJG2151	37·2	1131	0·0952	0·705388	27	86	0·705272	26·41	218·03	0·0732	0·512564	9	0·512523
Koffiefontein kimberlite	KK 3	82·3	816	0·2919	0·704587	16	90	0·704212	13·0	98·0	0·0802	0·512607	17	0·512560
Koffiefontein kimberlite	KK 6	29·6	1470	0·0583	0·704850	17	90	0·704775	16·7	129	0·0783	0·512607	16	0·512561
Lekkerfontein kimberlite	LKF 1	112·4	1810	0·1796	0·703564	18	74*	0·703375	26·28	190·03	0·0836	0·512633	12	0·512593
Monastery kimberlite	ROM312	93·9	1071	0·2537	0·703601	15	88	0·703284	16·21	110·46	0·0887	0·512673	10	0·512622
Wesselton kimberlite	C07	66·5	1088	0·1769	0·704527	17	84	0·704316	15·67	103·76	0·0913	0·512647	9	0·512597
Wesselton Floors' Sills	K119/2	62·9	2252	0·0808	0·704765	25	84	0·704669	33·13	239·53	0·0836	0·512613	9	0·512567
Wesselton Floors' Sills	K119/3	55·8	1468	0·1100	0·704755	16	84	0·704624	17·57	128·45	0·0827	0·512594	10	0·512549
Wesselton Floors' Sills	K5/1	108·1	1538	0·2034	0·704280	27	84	0·704037	36·12	247·26	0·0883	0·512671	9	0·512622
Group I kimberlites: off-craton														
Abbotsford E. kimberlite	JJG 3118	10·2	998	0·0296	0·704046	15	150*	0·703983	10·9	69·7	0·0945	0·512593	11	0·512500
Gansfontein kimberlite	GNF 2	80·0	1154	0·2007	0·704080	18	74*	0·703869	22·66	155·53	0·0881	0·512698	8	0·512655
Hebron kimberlite	HEB 1A	49·1	733	0·1938	0·703887	14	74*	0·703684	10·9	68·8	0·0958	0·512752	9	0·512705
Klipgatsfontein kimberlite	JAR 31012	12·1	876	0·0400	0·703906	15	74*	0·703864	14·8	96·4	0·0928	0·512720	9	0·512675
Klipgatsfontein kimberlite	JJG 4323	28·2	1010	0·0808	0·703917	15	74*	0·703832	15·9	102	0·0942	0·512723	10	0·512678
Uintjiesberg kimberlite	UB 1	46·4	1232	0·1090	0·704704	17	101	0·704548	24·8	171	0·0877	0·512602	10	0·512544
Uintjiesberg kimberlite	UB 6	38·9	1465	0·0768	0·704669	17	101	0·704559	19·1	131	0·0881	0·512582	8	0·512524
Zeekoegat kimberlite	JJG 1906	8·93	447	0·0578	0·704285	15	150*	0·704161	10·0	63·6	0·0950	0·512579	9	0·512485
Group II kimberlites: on-craton														
Bellsbank kimberlite	JJG 4676	120	1947	0·1784	0·708296	17	122	0·707988	21·5	224	0·0580	0·512051	9	0·512005
New Elands kimberlite	NE K6	163	1061	0·4448	0·708189	17	126	0·707394	16·2	139	0·0704	0·511972	8	0·511914
Newlands kimberlite	JJG 24	72·9	1000	0·2110	0·708161	18	114	0·707819	13·0	129	0·0609	0·512004	8	0·511958
Newlands kimberlite	JJG 24D	72·9	1000	0·2110	0·708155	14	114	0·707813						
Roberts Victor kimberlite	RVK 1	48·1	2396	0·0581	0·708241	16	128	0·708135	25·40	244·77	0·0627	0·511917	9	0·511864
Roberts Victor kimberlite	RVK 2	69·3	1529	0·1312	0·707633	18	128	0·707394	26·57	261·97	0·0613	0·511920	9	0·511869
Group II kimberlites: off-craton														
Brandewynskuil kimberlite	K6/11	103	1453	0·2052	0·708712	17	117*	0·708371	12·6	105	0·0637	0·511989	10	0·511934
Eendekuil kimberlite	K2/2	187	1438	0·3765	0·707862	17	110	0·707273	15·5	126	0·0744	0·512098	8	0·512045
Markt kimberlite	MRK 3	80·8	1677	0·1395	0·708606	16	117	0·708374	19·3	157	0·0743	0·512010	10	0·511953

Element concentrations of kimberlite samples are from ICP-MS (ppm) analyses or from le Roex *et al*. (2003) and Harris *et al*. (2004). Initial isotope (i) ratios were calculated using kimberlite emplacement ages (Ma) unless otherwise indicated (*), for which ages have been assumed. Ages from Allsopp & Barrett (1975), Davis (1977), Clement *et al*. (1979), Allsopp [unpublished, in Skinner (1989)], and Smith *et al*. (1994). Newlands kimberlite sample JJG 24D is a duplicate analysis of sample JJG 24. Decay constant for Rb–Sr isotope system $= 1{\cdot}42 \times 10^{-11}$ a^{-1} and measured isotope ratios are normalized to $^{86}Sr/^{88}Sr = 0{\cdot}1194$. Decay constant for Sm–Nd isotope system $= 6{\cdot}54 \times 10^{-12}$ a^{-1} and measured isotope ratios are normalized to $^{146}Nd/^{144}Nd = 0{\cdot}7219$.

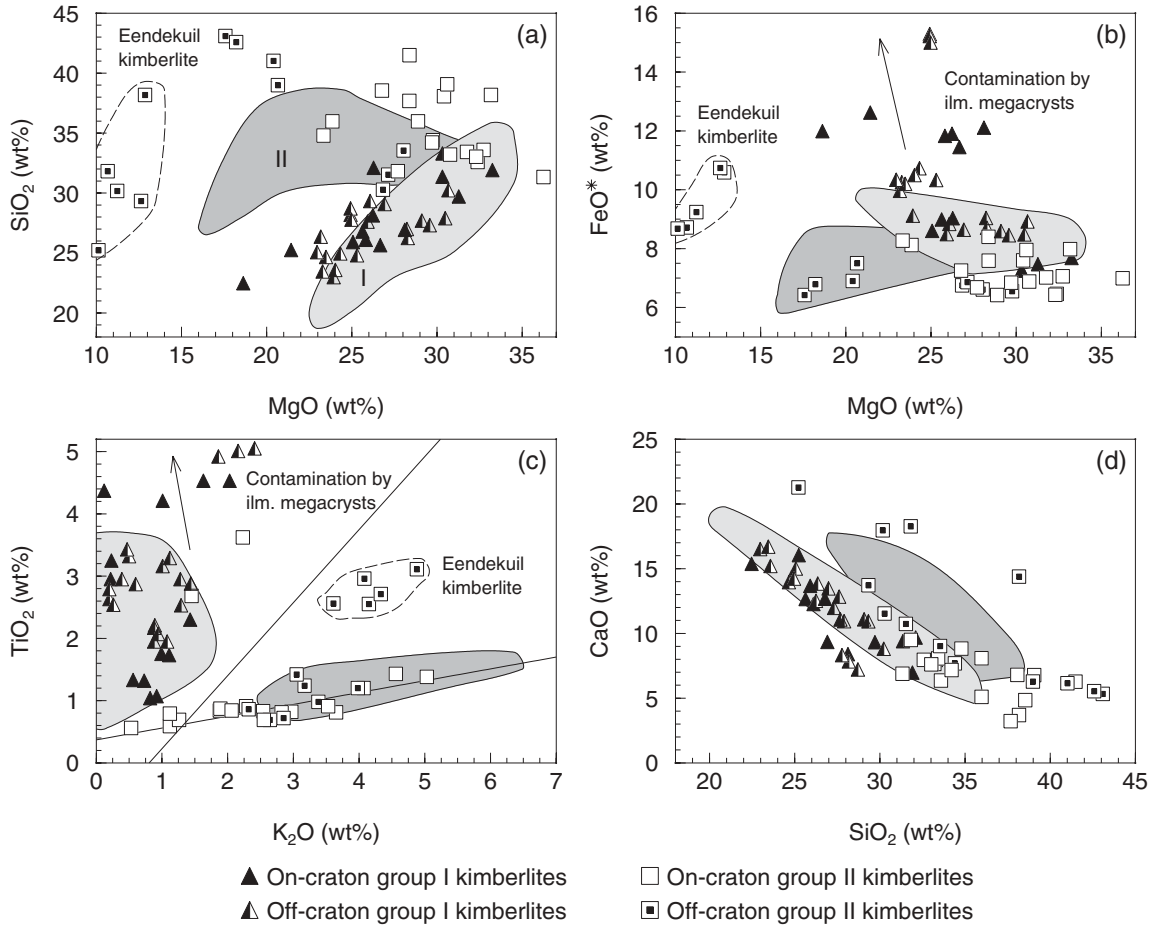

Fig. 2. Variation of (a) SiO_2 vs MgO, (b) FeO* vs MgO, (c) TiO_2 vs K_2O and (d) CaO vs SiO_2 in on- and off-craton Group I and Group II kimberlites. Symbols for off-craton Group I kimberlites include analyses from the Uintjiesberg kimberlite (Harris *et al.*, 2004). Dashed field represents the evolved Group II Eendekuil kimberlite. Light shaded field represents the on-craton Group I Kimberley kimberlites (le Roex *et al.*, 2003) and dark shaded field represents the on-craton Swartruggens and Star Group II kimberlites (Coe, 2004). Group I–Group II dividing lines in (c) are from Smith *et al.* (1985*b*).

contents varying from 22·5 to 33·3 wt %, whereas MgO varies between 18·6 and 33·3 wt %. On the whole, the more macrocrystic samples tend to have higher SiO_2 and MgO contents, and Mg-numbers (atomic $Mg/(Mg + Fe^{2+}) > 0{\cdot}85$), than the less macrocrystic samples (Mg-numbers = 0·76–0·85). FeO* (all iron as Fe^{2+}) concentrations vary from 7·5 to 15·3 wt % and tend to show a broad negative correlation with MgO (Fig. 2b). Samples from the Monastery, Lekkerfontein and Gansfontein kimberlites that have >11 wt % FeO* are interpreted to have been contaminated by ilmenite megacrysts, known to be abundant at these localities (Boyd & Nixon, 1975; Robey, 1981). It is also apparent that off-craton kimberlites tend to have lower SiO_2 and MgO, but higher FeO* than on-craton kimberlites (disregarding those kimberlites affected by ilmenite megacryst contamination), although still broadly falling within the field of on-craton Group I kimberlites.

The range in TiO_2 contents of the samples is greater than that for Al_2O_3 (1·0–5·1 wt % TiO_2 and 1·8–4·4 wt % Al_2O_3; Fig. 2c, Table 2), and samples fall generally within the field of the on-craton Kimberley kimberlites. Ignoring the possible effect of ilmenite megacryst contamination (e.g. TiO_2 >4 wt % in Gansfontein, Monastery and Lekkerfontein kimberlites), it is apparent that off-craton kimberlites have compositions that tend to plot towards the high TiO_2 end of the field of on-craton Group I kimberlites (Fig. 2c). The majority of the Group I kimberlite samples have low K_2O abundances (<1·5 wt %; Fig. 2c), except for a few outliers (1·6–2·4 wt % K_2O; Lekkerfontein, Monastery, Gansfontein kimberlites). A well-defined negative correlation exists between CaO and SiO_2 (Fig. 2d), whereas CO_2 (1·5–11·7 wt %) and CaO (7·0–16·7 wt %) are positively correlated (Table 2). Most off-craton kimberlites tend to have higher CaO and CO_2 than the on-craton kimberlites, although still broadly falling within the field of on-craton kimberlites.

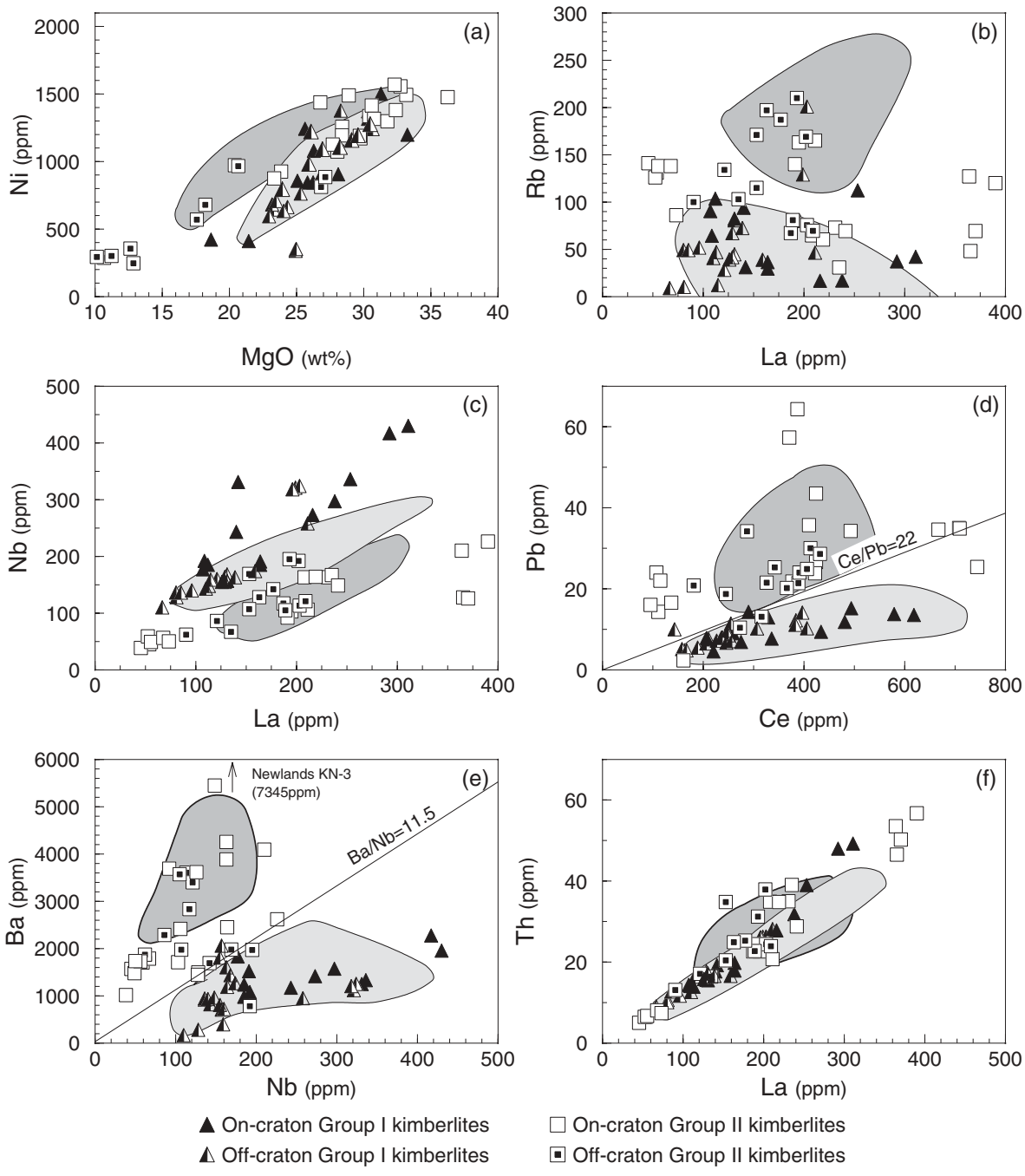

Fig. 3. Variation of (a) Ni vs MgO, (b) Rb vs La, (c) Nb vs La, (d) Pb vs Ce, (e) Ba vs Nb and (f) Th vs La in on- and off-craton Group I and Group II kimberlites. Dividing lines for Ce/Pb in (d) and Ba/Nb in (e) provide distinction between kimberlite groups. Symbols for off-craton Group I kimberlites include analyses from the Uintjiesberg kimberlite (Harris *et al.*, 2004). Light shaded field represents the on-craton Group I Kimberley kimberlites (le Roex *et al.*, 2003) and dark shaded field represents the on-craton Swartruggens and Star Group II kimberlites (Coe, 2004).

Transition metals show good positive correlations with MgO (e.g. Ni in Fig. 3a), with Ni varying between 340 and 1500 ppm, and Cr varying between 450 and 2028 ppm (Table 2). No significant differences between on- and off-craton kimberlites are apparent within this group of elements, although concentrations do show some correlation with olivine macrocryst content. Large ion lithophile element (LILE) concentrations are highly variable (e.g. 9–112 ppm Rb; 280–2276 ppm Ba) and show no correlation with the more immobile

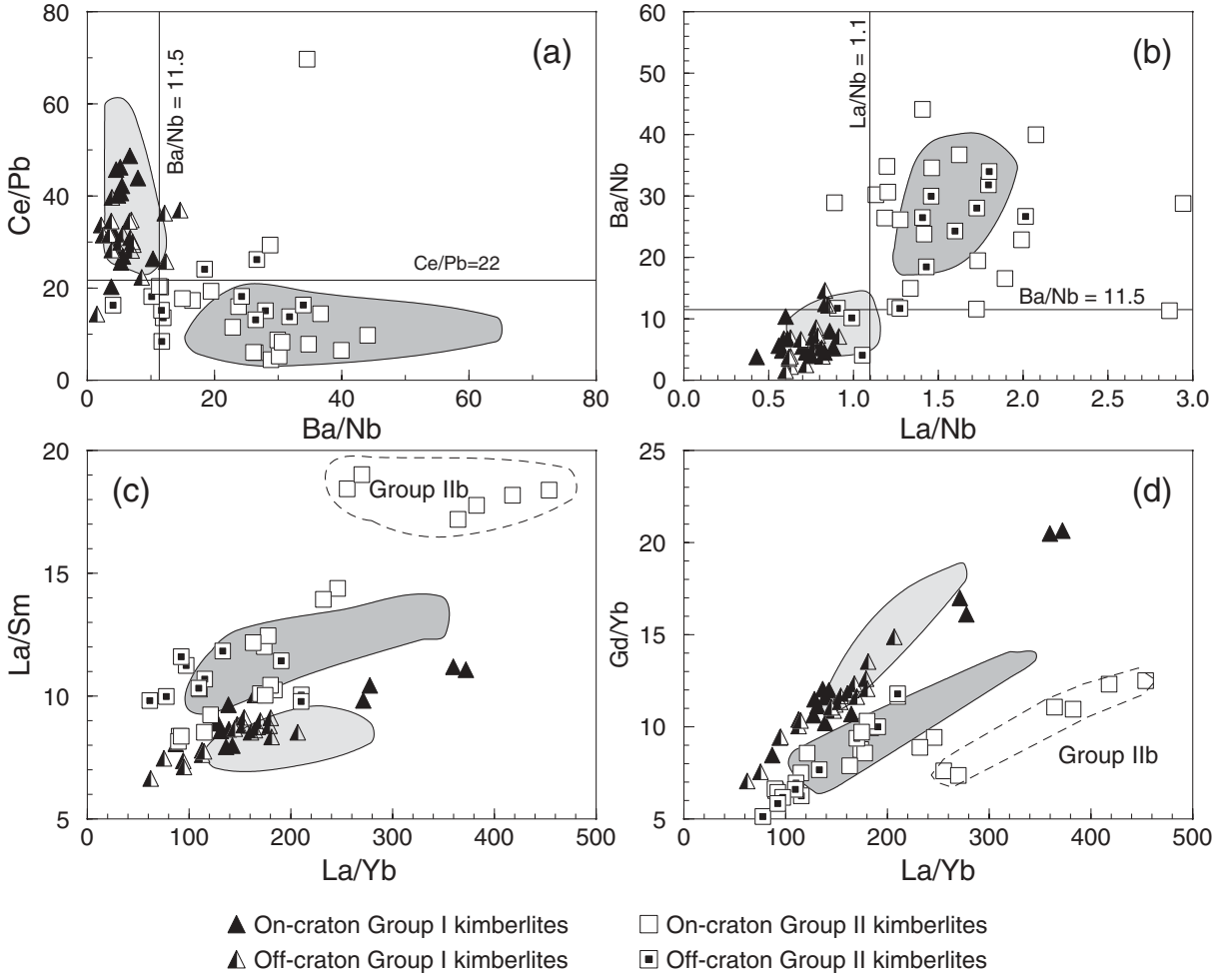

Fig. 4. Variation of (a) Ce/Pb vs Ba/Nb, (b) Ba/Nb vs La/Nb, (c) La/Sm vs La/Yb and (d) Gd/Yb vs La/Yb in on- and off-craton Group I and Group II kimberlites. Dividing lines for Ba/Nb, Ce/Pb and La/Nb in (a) and (b) provide distinction between kimberlite groups. Dashed field represents the Group IIb kimberlites. Light shaded field represents the on-craton Group I Kimberley kimberlites (le Roex *et al.*, 2003) and dark shaded field represents the on-craton Swartruggens and Star Group II kimberlites (Coe, 2004).

incompatible elements (e.g. La in Fig. 3b). Inter-element correlations of high field strength elements (HFSE; Zr, Nb and Hf) with other incompatible elements (e.g. La) are generally good over a wide range of concentrations (Fig. 3c). Inter-element ratios involving fluid-mobile elements are highly variable (e.g. K/Rb = 33–240; Ce/Pb = 14–49), whereas those involving the more immobile elements are more restricted (Figs 3 and 4; e.g. La/Nb = 0·7 ± 0·1; Th/Nb = 0·09 ± 0·02; Zr/Hf = 52 ± 6·6; Nb/Ta = 20 ± 5·6).

All of the analysed Group I kimberlites, both on- and off-craton, have broadly similar sub-parallel chondrite-normalized REE patterns (Fig. 5a), with considerable enrichment of the light REE (LREE; La = 300–1300 × chondrite) relative to the heavy REE (HREE; Lu = 3–8 × chondrite). In detail, La/Yb_N (44·7–267) and La/Sm_N (4·3–7·2) ratios are significantly variable. The analysed on- and off-craton kimberlites generally fall within the fields of the on-craton Kimberley and off-craton Uintjiesberg kimberlites, respectively (Fig. 5a), although it is evident from Fig. 4c and d that off-craton Group I kimberlites tend to have lower La/Sm, La/Yb and Gd/Yb ratios than some of their on-craton counterparts.

Primitive mantle-normalized trace element patterns are generally smooth, with strong enrichment in the more incompatible elements (e.g. Nb = 155–603 and Ba = 24–326 × primitive mantle), and relative depletions of Rb, K, Sr, Hf and Ti (Fig. 6a). These negative anomalies appear to be a characteristic feature of Group I kimberlites (le Roex *et al.*, 2003; Harris *et al.*, 2004). The magnitudes of the anomalies can be described by the X/X^* notation (where X is the normalized value and X^* the interpolated value calculated from the adjacent elements). Negative Rb and K anomalies tend to be larger (K/K* = 0·0–0·3; calculated using Th and La and not U because of its mobility) than the Ti anomalies

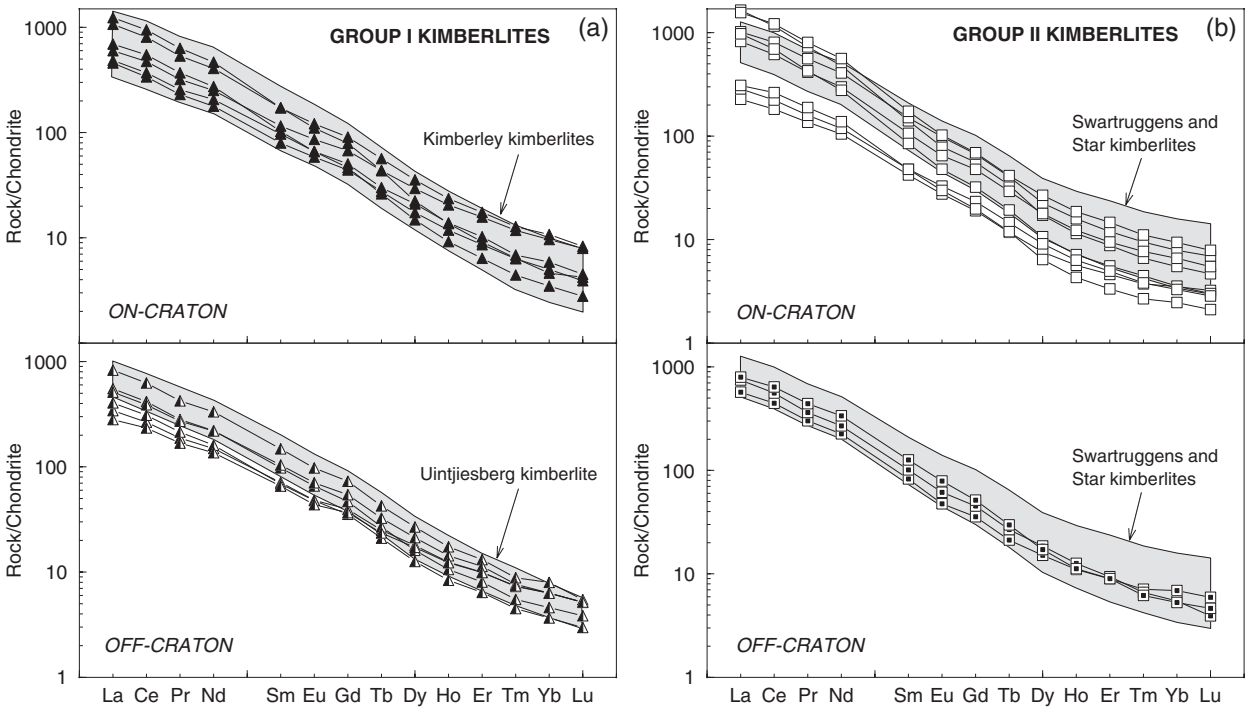

Fig. 5. Chondrite-normalized REE diagrams for on- and off-craton (a) Group I and (b) Group II kimberlites. Data for labelled fields are from le Roex *et al.* (2003), Coe (2004) and Harris *et al.* (2004). Normalizing values are from Sun & McDonough (1989).

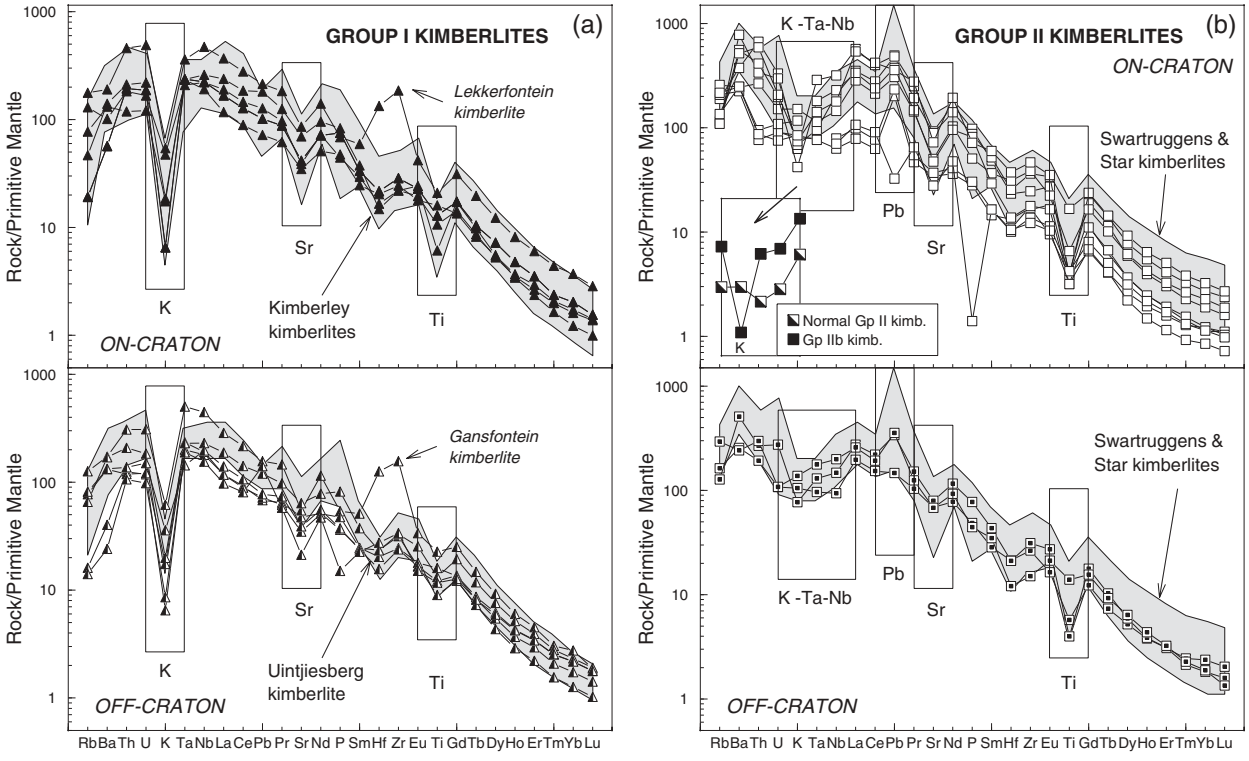

Fig. 6. Primitive mantle-normalized trace element patterns for on- and off-craton (a) Group I and (b) Group II kimberlites, with highlighted trace element anomalies. Data for labelled fields are from le Roex *et al.* (2003), Coe (2004) and Harris *et al.* (2004). Normalizing values are from Sun & McDonough (1989).

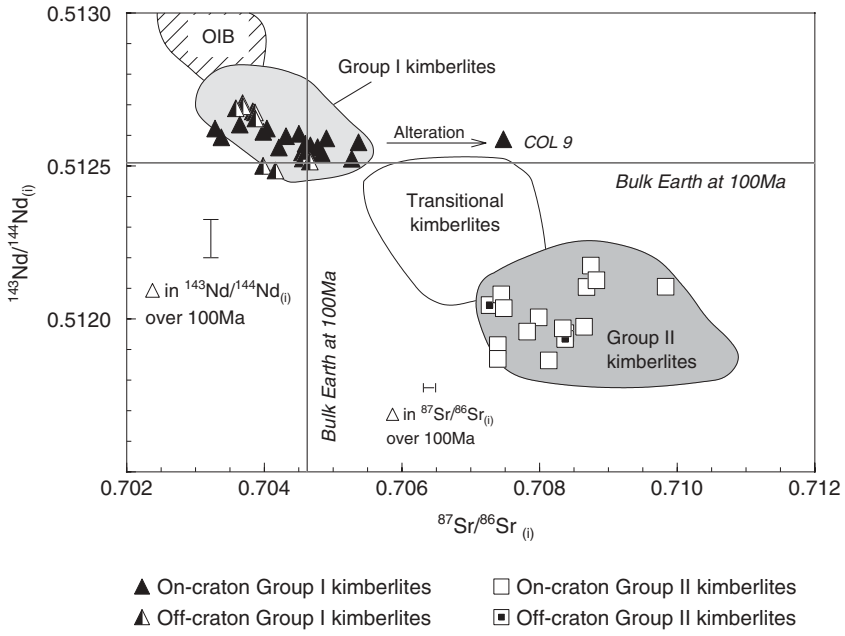

Fig. 7. Variation of initial $^{143}Nd/^{144}Nd$ and $^{87}Sr/^{86}Sr$ for on- and off-craton Group I and Group II analysed in this study (Table 3). Isotope data plotted for the Finsch and New Elands kimberlites analysed include data from Fraser & Hawkesworth (1992) and Smith (1983). Error bars for $^{143}Nd/^{144}Nd$ and $^{87}Sr/^{86}Sr$ represent the magnitude of the change in isotope ratios over 100 Myr. Initial isotope ratios are calculated according to the age or inferred age of intrusion and 2σ errors are less than the symbol size. Labelled shaded fields represent published data for South African Group I, Group II and Transitional kimberlites (Smith, 1983; Fraser & Hawkesworth, 1992; Tainton, 1992; Clark, 1994; Nowell *et al.*, 1999, 2004; Coe, 2004; Becker & le Roex, in preparation) and South Atlantic OIB (O'Nions & Pankhurst, 1974; O'Nions *et al.*, 1977; le Roex, 1985; le Roex *et al.*, 1990).

(Ti/Ti* = 0·3–1·0). In some instances (e.g. Koffiefontein kimberlite), the magnitudes of the anomalies increase with the level of incompatible element enrichment in individual samples. Minor negative Sr anomalies, as well as occasional negative Hf anomalies, are also features of the analysed Group I kimberlites. Rare, strongly positive Zr–Hf anomalies (Fig. 6a) are attributed to zircon megacryst contamination and partial assimilation (Lekkerfontein, Gansfontein and Monastery kimberlites).

Calculated initial $^{87}Sr/^{86}Sr$ and $^{143}Nd/^{144}Nd$ ratios of the Group I kimberlites from this study, as well as those analysed to complement the datasets presented by le Roex *et al.* (2003) and Harris *et al.* (2004), are reported in Table 3 and illustrated in Fig. 7. Initial $^{87}Sr/^{86}Sr$ ratios of the analysed Group I kimberlites vary from 0·70328 ± 2 to 0·70537 ± 2, whereas initial $^{143}Nd/^{144}Nd$ ratios vary between 0·51249 ± 1 and 0·51271 ± 1, and generally show good overlap with the field of southern African Group I kimberlites (Fig. 7). The strong displacement of the single sample COL 9 to high $^{87}Sr/^{86}Sr$ (Fig. 7) is attributed to alteration by crustal fluids. Although subtle differences exist in initial $^{87}Sr/^{86}Sr$ ratios between samples that may be related to the olivine macrocryst content (the more olivine macrocrystic samples tend to have higher $^{87}Sr/^{86}Sr_{(i)}$), no significant differences are evident between initial $^{87}Sr/^{86}Sr$ and $^{143}Nd/^{144}Nd$ ratios of on- and off-craton Group I kimberlites.

On- and off-craton Group II kimberlites

Although there is considerable scatter in the data, for a given MgO content the analysed Group II kimberlites are characterized by higher SiO_2 contents (29·0–43·1 wt %) than the Group I kimberlites (Fig. 2a); this feature is also shown by the on-craton Swartruggens and Star Group II kimberlites (Coe, 2004). Unlike the Group I kimberlites, there is no obvious correlation between MgO and SiO_2, although some within-pipe correlations do exist (e.g. Markt and Eendekuil kimberlites). Variation in MgO concentrations and Mg-number is large (MgO = 17·1–36·3 wt %; Mg-number = 0·80–0·91), with the more MgO-rich samples being more macrocrystic in character (e.g. Bellsbank, Newlands and Markt kimberlites). The off-craton Eendekuil kimberlite (argued later to be highly fractionated) falls outside these ranges, having substantially lower MgO and Mg-number (Fig. 2a; Table 2). FeO* contents mostly range from 6·4 to 8·0 wt % (Fig. 2b), with the evolved off-craton Eendekuil kimberlite being richest in FeO* (up to 11·5 wt %).

Most samples show low abundances of TiO_2 (0·56–1·4 wt %) and Al_2O_3 (0·79–4·5 wt %), but some (e.g. Eendekuil and Brandewynskuil kimberlites), argued later to show evidence for crustal contamination and crystal fractionation, tend to high TiO_2 (>2 wt %) and Al_2O_3 (>5 wt %). On the whole, the Group II kimberlites show distinctively lower TiO_2, but higher K_2O (up to 5 wt %)

than the Group I kimberlites (Fig. 2c), a characteristic feature noted by Smith *et al.* (1985*b*). The on-craton Newlands and Bellsbank Group II kimberlites have unusually low K_2O (0·53–1·9 wt %), and for reasons discussed later are referred to as Group IIb kimberlites. Good correlations exist between CaO (4·8–21·3 wt %), CO_2 (up to 15·1 wt %) and SiO_2 (Fig. 2d); for a given SiO_2 content Group II kimberlites tend to have higher CaO than Group I kimberlites. CaO and CO_2 concentrations in the analysed Group II kimberlites are more variable than in the Swartruggens and Star kimberlites (Fig. 2d). Other than off-craton Group II kimberlites having generally higher CaO for a given SiO_2 content, no other obvious differences are evident in the major element geochemistry of on- and off-craton Group II kimberlites.

The transition metals Ni (570–2062 ppm) and Cr (485–2326 ppm) show a wide range in abundance and correlate well with MgO (Fig. 3a) and Mg-number. Although the off-craton Group II kimberlites tend to have lower Ni than their on-craton counterparts, this might simply reflect the small size of the off-craton dataset and the unusually evolved Eendekuil kimberlite. Of perhaps more significance is that Group II kimberlites tend to have higher Ni concentrations, for a given MgO content than Group I kimberlites (Fig. 3a). LILE and Pb concentrations of Group II kimberlites show poor correlation with the more immobile incompatible elements (e.g. La; Fig. 3b), but are distinctively higher (31–210 ppm Rb; 780–7345 ppm Ba; 17–64 ppm Pb (Sanddrift sample K5/P2 excepted) than in Group I kimberlites (Table 2; Fig. 3).

Incompatible element ratios are particularly useful in distinguishing between Group I and Group II kimberlites, with the latter having significantly lower Ce/Pb (16 ± 12) and higher La/Nb (1·6 ± 0·5), Ba/Nb (24 ± 10) and Th/Nb (0·21 ± 0·06) (e.g. Table 2; Fig. 4). The high values for ratios involving Nb reflect the characteristic depletion in Nb (38–192 ppm) compared with Group I kimberlites (~100–400 ppm; Fig. 3). In contrast, inter-element ratios of other HFSE pairs (e.g. Zr/Hf = 47 ± 5; Nb/Ta = 25 ± 10) are not dissimilar to those of Group I kimberlites (Zr/Hf = 52 ± 6·6; Nb/Ta = 20 ± 5·6).

The chondrite-normalized REE patterns of the analysed Group II kimberlites are sub-parallel and characterized by extreme LREE enrichment (La up to 1600 × chondrite) relative to the HREE (Lu = 2–10 × chondrite; Fig. 5b), with most of the analysed samples falling in the field defined by the on-craton Swartruggens and Star Group II kimberlites; exceptions are Finsch, Middlewater and Sanddrift. La/Yb and La/Sm are generally high and illustrative of the steep LREE slope in chondrite-normalized diagrams (La/Yb_N = 44–180, La/Sm_N = 5·3–9·3), with the two on-craton Group IIb kimberlites (Bellsbank and Newlands) having appreciably higher La/Yb_N (183–300) and La/Sm_N (11·1–12·3) ratios (Fig. 4d). Of significance is that the Group II kimberlites have distinctly higher La/Sm and La/Yb ratios, but lower Gd/Yb ratios than Group I kimberlites (Fig. 4c and d).

Steep patterns, similar to the chondrite-normalized REE patterns, occur on primitive mantle-normalized trace element diagrams (Fig. 6b) with the analysed samples showing strong enrichment in incompatible elements (e.g. Ba = 112–779 and Th = 87–677 × primitive mantle). Superimposed on the generally smooth patterns, there are distinct relative depletions in Rb, Ti and Sr, enrichment in Pb and a broad depletion in the group of elements K–Ta–Nb (Fig. 6b), features that are common to the Swartruggens and Star Group II kimberlites (Coe, 2004). Samples from the Bellsbank and Newlands kimberlites are distinct in having a strong relative depletion in K ($K/K^* < 0·1$) and Rb (see insert to Fig. 6b), more akin to the Group I kimberlites (Fig. 6a). Consequently, as mentioned above, Group II kimberlites are subdivided into two varieties, Group II with subdued relative depletion in K, and Group IIb with strong relative depletion in K (and Rb). The Group IIb kimberlites also tend to have larger negative Ti anomalies ($Ti/Ti^* = 0·2–0·3$ vs 0·2–0·8). Positive Pb anomalies on primitive mantle-normalized diagrams are a feature of all but one (Sanddrift kimberlite, which also has a large negative P anomaly) of the analysed Group II kimberlites ($Ce/Pb_N < 1$; Fig. 6b), with some samples showing fairly large anomalies. The Swartruggens and Star Group II kimberlites are likewise relatively enriched in Pb (Fig. 6b). Most samples also show a minor relative depletion in Hf ($Sm/Hf_N < 2·0$), but in the Eendekuil kimberlite there is a much better developed distinct negative Zr and Hf anomaly ($Sm/Hf_N \sim 2·9$). Depletion in Ta and Nb is a ubiquitous feature of the analysed Group II kimberlites, as well as of the Swartruggens and Star Group II kimberlites (Coe, 2004) with La/Nb_N ratios generally being >1·3 (Table 2).

Initial $^{87}Sr/^{86}Sr$ ratios of the Group II kimberlites analysed in this study vary from 0·70728 ± 2 to 0·70837 ± 2, whereas initial $^{143}Nd/^{144}Nd$ ratios are characteristically unradiogenic and vary from 0·51186 ±1 to 0·51205 ± 1 (Table 3). No significant isotopic differences are evident between on- and off-craton Group II kimberlites. The co-variation of initial $^{143}Nd/^{144}Nd$ and $^{87}Sr/^{86}Sr$ ratios shows a scattered distribution that lies within the field previously defined for South African Group II kimberlites (Fig. 7), lying well within the 'enriched quadrant' (Smith, 1983; Fraser & Hawkesworth, 1992; Tainton, 1992; Nowell *et al.*, 1999, 2004; Coe, 2004).

PETROGENESIS

The volatile-rich and hybrid nature of kimberlite magmas requires that considerable care be given to

addressing contamination and alteration processes that might have compromised the kimberlite magma composition subsequent to leaving the source region (e.g. le Roex *et al.*, 2003). Before considering possible genetic models, we first consider the possible impact of such secondary processes on the geochemistry of the analysed samples.

Alteration and crustal contamination

The brecciated and permeable nature of kimberlites makes them prone to alteration (Berg & Allsopp, 1972), particularly as primary kimberlite magmas are volatile-rich. Alteration of the kimberlite can be both a primary (movement of crystallizing deuteric fluids) and a secondary (movement of meteoric waters) process. Not only do the kimberlites in this study show various petrographic features indicative of alteration (e.g. serpentinization or carbonatization), but these effects can also be identified in the major element geochemistry (e.g. loss of MgO and gain of volatiles during serpentinization), trace element geochemistry (e.g. lack of correlation of the mobile elements Rb and K with more immobile elements such as La; Fig. 3b) and isotope geochemistry (e.g. increase of $^{87}Sr/^{86}Sr$ ratios, Barrett & Berg, 1975; seen most strongly in sample COL 9). The HFSE are generally unaffected by such processes.

Similarly, because kimberlites commonly entrain numerous crustal xenoliths, the degree of assimilation of country rock and its effect on bulk-rock geochemistry needs to be considered. The effects of crustal contamination (e.g. increase in SiO_2, Al_2O_3 and Na_2O, and decrease in MgO) can be partially quantified with the contamination index (C.I.) of Clement (1982), or qualitatively recognized using parameters identified by le Roex *et al.* (2003; e.g. raised HREE patterns, raised Pb in Group I kimberlites). Most Group I and Group II kimberlites in this study have a C.I. near unity and less than 1·5, respectively, i.e. classify as being uncontaminated.

Through careful initial sampling and removal of all visibly altered or veined material and xenolith fragments, the effects of alteration and contamination have been minimized. Furthermore, by applying the geochemical criteria listed by le Roex *et al.* (2003), in combination with Clement's (1982) C.I., those analysed compositions that appear to have been severely compromised either are excluded from the following petrogenetic discussions or are specifically mentioned. The interpretation of the geochemistry of the remaining samples is done with caution, with reference being made to occasions when alteration or contamination still needs to be borne in mind.

Macrocryst entrainment

Macrocrysts entrained by kimberlites are typically anhedral with strained physical characteristics that suggest they are xenocrysts, derived from disaggregated mantle peridotite xenoliths (Clement *et al.*, 1984; Shee, 1985). Consequently, macrocrystic kimberlites are generally considered to be aggregates of mantle minerals as opposed to true liquid compositions (le Roex *et al.*, 2003). A number of previous studies (e.g. Fraser & Hawkesworth, 1992; Beard *et al.*, 2000; le Roex *et al.*, 2003; Coe, 2004; Harris *et al.*, 2004) have demonstrated that some of the variation in kimberlite bulk-rock geochemistry can be attributed to the entrainment of xenoliths of mantle peridotite; this is also true for the present study.

To consider only liquid compositions, the effect of macrocryst entrainment has to be addressed for each kimberlite sample. The regional nature of this study has resulted in few of the kimberlites being sampled in sufficient detail to evaluate evolutionary trends and the effect of peridotite entrainment, within a single kimberlite locality, as has been done in other kimberlite studies (e.g. Harris *et al.*, 2004). Consequently, what we have done is to assume that all the olivine macrocrysts in a particular sample are derived from disaggregated garnet lherzolite xenoliths [using an average composition calculated from Grégoire *et al.* (2003)]. Using proportions based on the estimated modal olivine abundance in the kimberlite sample, an equivalent proportion of garnet lherzolite was accordingly subtracted. In view of the inherent errors in estimating modal abundances, this correction procedure was applied only to samples with >10% modal olivine macrocrysts. Compatible trace elements were corrected using an average composition of garnet lherzolite (Grégoire *et al.*, 2003), whereas incompatible trace elements were effectively enriched in abundance by the proportion of lherzolite removed (assuming $D = 0$ for all elements). Although only an approximation, the very low partition coefficients and low incompatible element abundances in garnet lherzolite do not warrant a more complex approach. Given the broad range in $^{87}Sr/^{86}Sr$ and $^{143}Nd/^{144}Nd$ of mantle xenoliths entrained by South African kimberlites (e.g. Erlank *et al.*, 1987; Walker *et al.*, 1989; Pearson & Nowell, 2002), as well as the particularly low Nd concentrations in mantle peridotites (<5 ppm Nd), the isotopic compositions of the kimberlites have been left unchanged.

Fractional crystallization

Crystal fractionation *en route* to the surface or during shallow emplacement and cooling of the kimberlite magma will affect the composition of the primary kimberlite magma. Fractionation of olivine and phlogopite, and possibly calcite, have been proposed, based on detailed studies of individual kimberlites (e.g. Beard *et al.*, 2000; le Roex *et al.*, 2003; Coe, 2004; Harris *et al.*, 2004). Evolved, aphanitic kimberlite, in particular, is a good

example of the end product of such fractionation processes (le Roex *et al.*, 2003). Crystal fractionation/accumulation may have occurred to variable degrees, for example via flow differentiation, in macrocryst-bearing kimberlites (e.g. the evolved Eendekuil kimberlite).

On the basis of a number of lines of evidence, le Roex *et al.* (2003) and Harris *et al.* (2004) have argued that the ubiquitous negative anomalies in K, Rb, Sr and Ti in primitive mantle-normalized trace element diagrams are not related to crystal fractionation processes, but are features of the primary magmas of the Group I Kimberley and Uintjiesberg kimberlites. Following the arguments presented by le Roex *et al.* (2003) and Harris *et al.* (2004), we suggest that the ubiquitous negative Rb, K and Ti anomalies on primitive mantle-normalized trace element diagrams for the Group I kimberlites in this study are not the result of extensive phlogopite (Rb, K, Ti), ilmenite (Ti) or perovskite (Ti) fractionation (the last is supported also by the absence of an associated negative Nb and Ta anomaly), but are features of the primary kimberlite magmas. However, it is recognized that minor amounts of fractionation, as well as K and Rb mobility, may have an influence on the magnitudes of the anomalies.

Even though Nb and Ta are depleted in Group II kimberlites, the characteristic paucity of ilmenite and perovskite as groundmass phases (e.g. Skinner, 1989) argues against fractionation of a Ti-phase as the cause of the ubiquitous negative Ti anomaly and relative depletion in Nb and Ta in primitive mantle-normalized trace element patterns. Based on similar calculations to those used by le Roex *et al.* (2003) and Harris *et al.*, (2004), it can be argued that relative depletion in Rb, K, Sr, Ti, Nb and Ta is a primary feature of normal Group II and Group IIb kimberlites in this study, not caused by the fractional crystallization of phlogopite (K, Ti; Coe, 2004). Furthermore, the strong relative depletion in K and Rb present in the Group IIb kimberlites is argued here not to be due to phlogopite fractionation, but to be a feature inherited from the mantle source region.

Composition of close-to-primary kimberlite magmas

To allow meaningful and regional inter-group comparison of the geochemistry of on- and off-craton Group I and Group II kimberlites, it is important to identify a representative composition for each kimberlite that is close-to-primary in character. Because of the hybrid nature of kimberlites, and as no examples of quenched kimberlite exist (Mitchell, 2004), aphanitic kimberlite has been considered a proxy for a primary magma (Edgar & Charbonneau, 1993; Price *et al.*, 2000). More recently, le Roex *et al.* (2003) and Harris *et al.* (2004) have constrained the compositions of primary kimberlite magmas by using the trajectories between macrocrystic and aphanitic kimberlite on major element variation diagrams. However, owing to the regional nature of this study, primary kimberlite magma compositions cannot be constrained here using similar methods, as sufficient samples are not available from each locality. Here we define close-to-primary kimberlite magma compositions as those being least affected by alteration, crustal contamination and fractional crystallization, and, specifically, having been corrected for macrocryst entrainment where necessary (as described earlier). Not every kimberlite represents a close-to-primary magma (e.g. aphanitic Lekkerfontein kimberlite) and in a few cases (e.g. Pampoenpoort, Jonkerwater, Middlewater and Sandrift kimberlites, where samples were made available as powders from De Beers) the absence of thin sections prohibited any correction for macrocryst content; these samples are omitted from further discussion.

Inferred close-to-primary magma compositions of Group I kimberlites analysed in this study have ~22–28 wt % MgO, ~21–30 wt % SiO_2, 2·2–3·1 wt % Al_2O_3, ~10–17 wt % CaO, ~5·0–14 wt % CO_2, ~0·2–1·7 wt % K_2O and 660–1190 ppm Ni, with Mg-number varying between 0·82 and 0·87; these are broadly similar to primary Group I kimberlite compositions proposed in other studies (Price *et al.*, 2000; le Roex *et al.*, 2003; Harris *et al.*, 2004). Group II kimberlites in this study have close-to-primary magma compositions with ~28–38 wt % SiO_2, ~23–29 wt % MgO, ~1·0–4·3 wt % Al_2O_3, ~1·6–4·6 wt % K_2O, 8·1–13 wt % CaO, 1·3–7·4 wt % CO_2 and 590–1410 ppm Ni, with Mg-number between 0·86 and 0·89. The close-to-primary compositions of the analysed Group II kimberlites are similar to those of the Swartruggens and Star Group II kimberlites (Coe, 2004), but tend be slightly more Mg-rich and less K_2O-rich.

Inferred close-to-primary Group I kimberlite magma compositions from this study are also broadly consistent with experimental 'kimberlite' compositions (20–36 wt % SiO_2, 1·8–3·2 wt % Al_2O_3, 26–30 wt % MgO), obtained from low-degree melting of a carbonated lherzolite by Dalton & Presnall (1998*a*), except that the CaO content of the experimental kimberlites is significantly higher (15–31 wt %). The MgO and SiO_2 contents of inferred close-to-primary Group II kimberlites in this study also show some overlap with experimental compositions produced by <1% partial melting of a carbonated lherzolite at 6 GPa (Dalton & Presnall, 1998*a*).

Table 4 gives average Group I and Group II close-to-primary kimberlite magma compositions for major and trace elements and selected incompatible element ratios, calculated using data from this study and the literature (le Roex *et al.*, 2003; Coe, 2004; Harris *et al.*, 2004). There is considerable scatter around the averages (as reflected by the reported standard deviations), but nevertheless

Table 4: Average compositions and associated standard deviations of close-to-primary Group I and Group II kimberlites from South Africa

	Group I kimberlite		Group II kimberlite	
	Average	1 SD	Average	1 SD
SiO_2	26·15	2·7	33·89	4·8
TiO_2	2·58	0·7	1·77	1·5
Al_2O_3	2·76	0·45	3·76	2·0
Fe_2O_3	10·72	1·2	8·76	0·6
MnO	0·19	0·03	0·18	0·05
MgO	25·20	2·1	23·15	4·2
CaO	13·26	2·2	9·96	2·0
Na_2O	0·16	0·14	0·25	0·24
K_2O	0·83	0·46	3·63	1·4
P_2O_5	2·04	1·2	1·85	0·8
SO_3	0·17	0·15	0·21	0·16
NiO	0·11	0·03	0·14	0·06
Cr_2O_3	0·18	0·04	0·23	0·09
LOI	14·71	1·9	10·75	3·8
H_2O^-	0·66	0·27	1·34	1·7
Total	99·71		99·41	
H_2O^+	6·67	2·0	7·33	2·4
CO_2	8·19	2·9	4·21	2·8
Mg-no.	0·84	0·02	0·85	0·02
Zr	371	98	399	194
Nb	239	147	165	88
Co	89·1	9	74·7	9
Cr	1508	481	2096	449
Ni	935	235	977	298
V	155	46	112	46
Cu	95·9	60	42·9	14
Sc	17·4	4	25·4	7
Rb	47·1	25	151	57
Sr	1295	444	1869	671
Y	20·5	6	20·9	9
Ba	1380	876	3799	1503
La	181	106	298	183
Ce	358	211	576	343
Pr	38·3	22	59·0	34
Nd	144	78	204	109
Sm	20·0	9	22·2	10
Eu	5·07	2	5·04	2
Gd	13·1	5	12·3	5
Tb	1·41	0·5	1·36	0·6
Dy	5·81	2	5·45	2
Ho	0·85	0·3	0·84	0·4
Er	1·82	0·5	1·92	0·9
Tm	0·20	0·1	0·23	0·1
Yb	1·04	0·3	1·31	0·6
Lu	0·13	0·03	0·17	0·07
Hf	6·94	1	9·08	4
Ta	11·6	5	8·05	4
Pb	10·4	5	33·3	12
Th	24·3	18	40·3	27
U	5·76	4	6·14	3
Ba/Nb	5·7	2	25	8
La/Nb	0·75	0·1	1·8	0·5
Ce/Pb	34	7	17	7
$(La/Sm)_N$	5·6	0·8	8·2	2
$(La/Yb)_N$	124	62	168	86

Data from this study, le Roex *et al*. (2003), Coe (2004) and Harris *et al*. (2004). Mg-number calculated assuming $Fe_2O_3/FeO = 0·15$. Normalizing values from Sun & McDonough (1989).

certain elements stand out as being significantly different between the two kimberlite varieties. These include higher TiO_2, Fe_2O_3, MgO and CaO, and lower SiO_2 and K_2O in Group I kimberlites, and substantially higher Ba, Rb and Pb, and lower Nb and Ta in Group II kimberlites compared with Group I kimberlites. Although less marked, NiO appears to be slightly higher in Group II kimberlites on average than in Group I kimberlites (Table 4). It is argued later that these differences are inherited from their respective source regions.

Partial melting models

Experimental studies have shown that Group I kimberlite-like magmas can be produced by low degrees of partial melting of a carbonated garnet peridotite mantle source at ~3–8 GPa (Eggler & Wendlandt, 1979; Canil & Scarfe, 1990; Dalton & Presnall, 1998*a*) and that a continuum exists between carbonatitic and kimberlitic melts, with the transition between these magma types taking place between 0 and 1% melting (Dalton & Presnall, 1998*a*). Ulmer & Sweeney (2002) have also shown that Group II kimberlites could be formed by partial melting of a carbonated garnet harzburgite or lherzolite at pressures up to 10 GPa.

The characteristic incompatible element enrichment and fractionated REE patterns of kimberlites are consistent with derivation by very low degrees of partial melting of metasomatically enriched sources (e.g. Wass & Rogers, 1980). Partial melting is generally inferred to take place in

the presence of residual garnet because of the characteristic low HREE abundances and fractionated HREE patterns in both on- and off-craton kimberlites relative to typical mid-ocean ridge basalt (MORB; Rogers *et al.*, 1992; Tainton & McKenzie, 1994; le Roex *et al.*, 2003). Metasomatized lherzolite xenoliths from the Kaapvaal craton typically contain clinopyroxenes that have been enriched in the LREE (van Achterbergh *et al.*, 2001; Grégoire *et al.*, 2003) and therefore clinopyroxene is likely to be the major mineral host of these elements during partial melting. The semi-quantitative modelling of kimberlite source compositions outlined below is, therefore, based on a source comprising metasomatized garnet lherzolite and very low degrees of partial melting ($F < 2\%$). Some workers have argued that in view of the absence of olivine and orthopyroxene as liquidus phases during the experimental melting of kimberlites and lamproites, the source of such magmas is not a lherzolite (Foley, 1992*a*; Edgar & Charbonneau, 1993; Girnis *et al.*, 1995; Mitchell, 2004), but rather some more exotic mineral assemblage (e.g. clinopyroxene–phlogopite veins; Foley, 1992*b*); this possibility is also explored.

In view of the assumptions required to estimate primary kimberlite magma compositions, complex inversion modelling (e.g. Tainton & McKenzie, 1994) is not justified. Furthermore, given the number of assumptions that need to be made when modelling mantle melting processes, and to allow possible differences between the sources of Group I and Group II kimberlites, as well as on- and off-craton kimberlites to be recognized, it is necessary to restrict at least some of the variables. First, close-to-primary magma compositions were used together with a fixed degree ($F = 1\%$) of partial melting. Modal analyses of peridotite xenoliths entrained by on- and off-craton kimberlites (Mathias *et al.*, 1970; Maaloe & Aoki, 1977; Boyd & Mertzman, 1987; Franz *et al.*, 1996; Grégoire *et al.*, 2003; Boyd *et al.*, 2004) tend to be broadly similar, particularly with regard to the proportion of modal garnet (3–9 vol. %); consequently, we have assumed a fixed modal mineralogy for both on- and off-craton source regions. Semi-quantitative forward modelling of batch melting is based on the residual source mineralogy to avoid having to assume the reaction coefficients of the melting equation, using the partition coefficients summarized by le Roex *et al.* (2003).

Considering the unusual composition of kimberlites, the choice of suitable partition coefficients is limited to a silica-undersaturated system such as those for basaltic, carbonatitic or ultrapotassic melts (e.g. Schmidt *et al.*, 1999); none of which are ideal for kimberlites. Partition coefficients for basalts were chosen for modelling for both Group I and Group II kimberlites, because of their availability as a coherent dataset of elements. Differences in the CO_2 content of close-to-primary Group I (0·2–1·7%) and Group II kimberlites (1·3–7·4%) were not considered large enough to justify the use of carbonatitic partition coefficients for Group II kimberlites.

The observation that Group II kimberlites have on average steeper LREE (higher La/Sm), but flatter HREE slopes (lower Gd/Yb) than Group I kimberlites (Fig. 4), could imply differences in the source mineralogy. However, calculated melting trajectories (Fig. 8) illustrate that increasing the degree of partial melting decreases La/Sm and Gd/Yb, but cannot account for the differences between the kimberlite groups. Rather, it appears that Group II kimberlites are derived from sources with slightly higher La/Sm but lower Gd/Yb than Group I kimberlites. Given the difference in partition coefficients between La, Sm, Gd and Yb, this is consistent with derivation of Group II kimberlites from a source with less residual garnet but more residual clinopyroxene than that giving rise to Group I kimberlites. The residual modal mineralogy used for subsequent modelling is 67% olivine, 26% orthopyroxene, 3% garnet, 4% clinopyroxene for the Group I kimberlites. The residual modal mineralogy used for Group II kimberlites has the same olivine and orthopyroxene proportions (67% ol; 26% opx) as for Group I kimberlites but with less garnet (1%) and more clinopyroxene (6%). Although the measured La/Sm and Gd/Yb ratios of Kaapvaal garnet lherzolite xenoliths are variable, and show little correlation with the proportion of modal garnet or clinopyroxene (van Achterbergh *et al.*, 2001; Grégoire *et al.*, 2003; Simon *et al.*, 2003), the values used in the modelling and shown in Fig. 8 fall within the observed ranges.

Source region characteristics

Calculated compositions of mantle source regions in equilibrium with close-to-primary Group I kimberlites are all enriched in the LREE (4–25 × chondrite) and only slightly enriched in the HREE relative to chondrite (1·8–3·6 × chondrite; Fig. 9a). They have $La/Sm_N = 2·3–3·9$ and $La/Yb_N = 1·9–11·5$, but are depleted in the less incompatible elements relative to primitive mantle (Yb = 0·5–1 × primitive mantle; Fig. 9b). Similarly, calculated sources are also enriched in the more incompatible elements relative to primitive mantle (e.g. Th = 1–9 × primitive mantle). In the absence of residual phases capable of fractionating individual elements, the negative anomalies present in the close-to-primary magma compositions are transferred to the predicted source regions (Fig. 9b). Consequently, the calculated sources have negative Rb, Sr, K and Ti anomalies ($K/K^* < 0·2$; $Ti/Ti^* = 0·2–0·7$), as well as more subdued negative Hf anomalies. Predicted source compositions generally show good overlap with those calculated for the Group I on-craton Kimberley kimberlites and off-craton Uintjiesberg kimberlite (Harris *et al.*, 2004). Calculated source compositions overlap the field of garnet lherzolites from the

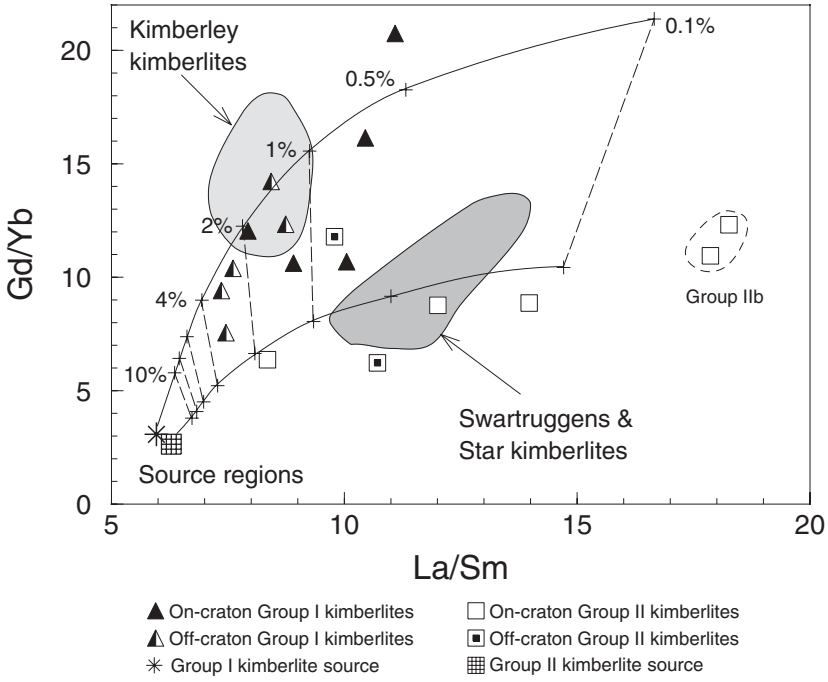

Fig. 8. Gd/Yb vs La/Sm for on- and off-craton Group I and Group II close-to-primary kimberlite magmas, including the Uintjiesberg kimberlite (Harris *et al.*, 2004). Dashed field represents the Group IIb kimberlites. Illustrated curves represent melting trajectories of inferred Group I and Group II kimberlite source regions (La/Sm = 6·0; Gd/Yb = 3·0 and La/Sm = 6·4; Gd/Yb = 2·5, respectively). Residual modal mineralogy as follows: Group I, ol:opx:cpx:gt = 0·67:0·26:0·04:0·03; Group II, ol:opx:cpx:gt = 0·67:0·26:0·06:0·01. Numbers shown represent the degree of melting. Shaded fields represent the on-craton Group I Kimberley (le Roex *et al.*, 2003) and on-craton Group II Swartruggens and Star kimberlites (Coe, 2004).

Kaapvaal craton for all elements other than K, which is significantly more depleted in the predicted sources than in peridotites (Fig. 9b). However, many of the peridotites from the study of Grégoire *et al.* (2003) contain modal phlogopite and are thus likely to have elevated K concentrations.

Because both on- and off-craton source compositions are calculated using the same parameters, any differences in the respective kimberlite magma compositions will be transferred to the sources. Consequently, predicted source compositions of off-craton Group I kimberlites appear to have lower La/Sm, La/Yb and Gd/Yb than on-craton Group I kimberlites. Alternatively, if the on- and off-craton sources were compositionally similar, then the off-craton kimberlites formed by slightly higher degrees of partial melting, as all Group I kimberlites fall roughly on the same melting trajectory (Fig. 8).

Predicted source regions in equilibrium with close-to-primary Group II kimberlite magmas are all enriched relative to chondrite, with the LREE (5–37 × chondrite) being considerably more enriched than the HREE (0·9–2·6 × chondrite; Fig. 9c). The sources of the Group IIb kimberlites are more enriched in the incompatible elements with higher La/Sm and La/Yb ($La/Sm_N \sim 6·9$) than those of normal Group II kimberlites (La/Sm_N = 3·2–5·4), suggesting that they are possibly lower degree partial melts than some of the other Group II kimberlites analysed in this study (Fig. 8). Calculated sources are also enriched in the highly incompatible LILE and HFSE and depleted in the less incompatible elements, relative to primitive mantle (e.g. Th = 1–11 × primitive mantle and Yb = 0·3–0·8 × primitive mantle, respectively; Fig. 9d). Negative Rb, K and Ti anomalies are larger for the sources of Group IIb kimberlites (K/K* ∼0·1, Ti/Ti* ∼0·2) than normal Group II kimberlites (K/K* = 0·3–1·0, Ti/Ti* = 0·2–0·6). All Group II kimberlite source regions show subdued depletion in Sr, Ta and Nb (La/Nb_N = 1·5–3·9), and slight enrichment in Pb (Ce/Pb_N = 0·2–1·0). Calculated source compositions (Fig. 9d) fall within the field of garnet lherzolite xenoliths from Grégoire *et al.* (2003). There appear to be no significant differences in calculated source compositions between on- and off-craton Group II kimberlites.

A number of recent studies of kimberlite petrogenesis based on bulk-rock geochemistry (Tainton & McKenzie, 1994; Beard *et al.*, 1998; Beard *et al.*, 2000; le Roex *et al.*, 2003; Chalapathi Rao *et al.*, 2004; Coe, 2004; Harris *et al.*, 2004) have all argued that the source regions of kimberlites have (at least) a two-stage evolutionary history, comprising initial melt-depletion with subsequent metasomatic enrichment in incompatible elements. Close-to-primary magmas of on- and off-craton Group I and

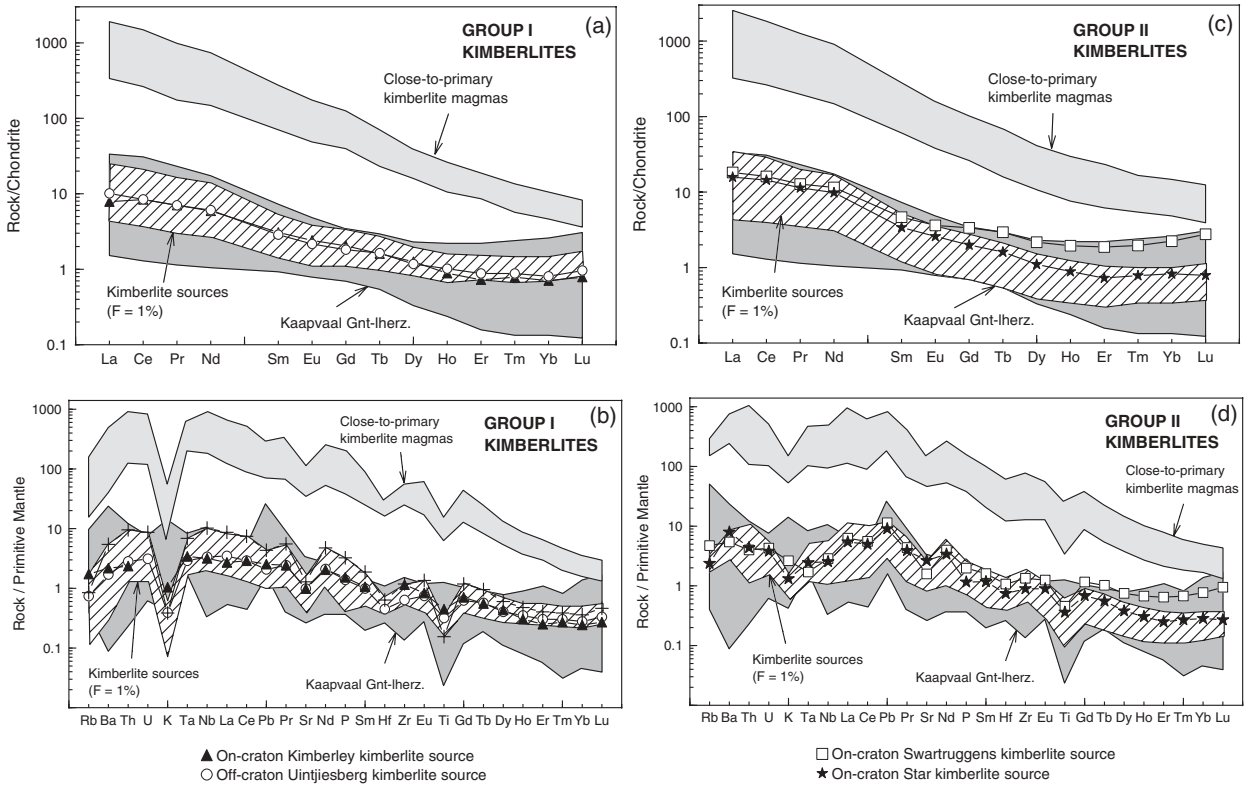

Fig. 9. Calculated chondrite- and primitive mantle-normalized source compositions of on- and off-craton Group I and Group II kimberlites, calculated by semi-quantitative forward modelling from close-to-primary kimberlite magmas assuming $F = 1\%$ and residual source region mineralogy as in Fig. 8. Calculated source compositions of the on-craton Group I Kimberley kimberlites (le Roex *et al.*, 2003), off-craton Group I Uintjiesberg kimberlite (Harris *et al.*, 2004) and on-craton Swartruggens and Star Group II kimberlites (Coe, 2004) are shown for comparison. Dark shaded field represents garnet lherzolite xenoliths from the Kaapvaal craton (Grégoire *et al.*, 2003). Normalizing values are from Sun & McDonough (1989).

Group II kimberlites all have high Mg-numbers (Mg-number = 0·82–0·89) and compatible trace element concentrations (e.g. 650–1400 ppm Ni) that suggest equilibration with residual olivine of $Fo_{92–96}$, having more than 2000 ppm Ni [calculated using $K_D^{Fe–Mg} = 0·34–0·36$ (Herzberg & O'Hara, 2002) and D_{Ni} from Beattie *et al.* (1991)]. It is notable that the calculated compositions of residual olivine in equilibrium with close-to-primary kimberlites tend to be more similar to refractory olivine included in diamonds than to olivine from Kaapvaal peridotite xenoliths (e.g. Phillips *et al.*, 2004). All kimberlites have low Al_2O_3 and Sc concentrations, as well as relative depletion in the HREE and fractionated HREE patterns indicative of the role of residual garnet, and suggest derivation from previously depleted mantle source regions (Tainton & McKenzie, 1994). Studies of peridotite xenoliths from the Kaapvaal craton and surrounding Proterozoic mantle have recognized that the SCLM beneath southern Africa has a depleted or infertile character, deficient in Fe, Ca and Al in comparison with oceanic mantle; additionally the Archaean mantle is more refractory than the younger Proterozoic mantle (Boyd & McCallister, 1976; Boyd & Mertzman, 1987; Boyd *et al.*, 2004). Given the apparent initial depleted character of kimberlite source regions, we concur with Tainton & McKenzie (1994), le Roex *et al.* (2003) and Harris *et al.* (2004), who have argued that they are more likely to be located within the SCLM than within the convecting asthenosphere.

Residual accessory phases

As forward modelling is based on a residual garnet lherzolite source with no accessory phases present, bulk partition coefficients for Rb, K, Ti, Sr and Nb during partial melting are all substantially less than unity; thus any anomalies in the close-to-primary kimberlite magmas are transferred to their source regions. Although some workers have argued for the presence of a residual K-bearing phase during partial melting to be the cause of negative K anomalies in some other alkaline magmas (e.g. Rogers *et al.*, 1992; Späth *et al.*, 2001; Williams *et al.*, 2004), others such as le Roex *et al.* (2003) and Harris *et al.* (2004) have argued that these are primary features of kimberlite source regions.

Notwithstanding the possible superimposed effect of low-temperature element mobility, evaluation of the ubiquitous negative Rb and K anomalies in the Group I kimberlites analysed in this study leads us to the same conclusion regarding the origin of the apparent depletion in these elements, i.e. that it is a primary source feature, and does not result from buffering by residual phlogopite. The role of residual phlogopite in Group II kimberlites is more ambiguous. Unlike Group I kimberlites, the absolute K content of Group II kimberlites is consistent with the presence of residual phlogopite (based, for example, on stoichiometry considerations and melting modes; Späth *et al.*, 2001), although most show only a minor relative depletion in K, suggesting that if present initially, phlogopite was fully or close to fully consumed during melting. This is consistent with the experimental evidence that phlogopite is not stable on the Group II kimberlite liquidus during melting in the presence of carbonate at pressures greater than 4–6·5 GPa, but rather breaks down to form garnet, orthopyroxene and a K-rich liquid (Yamashita *et al.*, 1995; Ulmer & Sweeney, 2002). An exception to this generalization might be the Group IIb kimberlites that show strong relative depletion in K (Fig. 6b). The radiogenic $^{87}Sr/^{86}Sr$ character of Group II kimberlites is consistent with the presence of phlogopite in the source.

Group II kimberlites show a distinct, and characteristic, depletion in Nb and Ta relative to elements of similar incompatibility (e.g. Fig. 6b), which suggests possible buffering against a residual titanate phase, such as rutile. Because rutile is typically a metasomatic phase (Haggerty, 1987), it is likely to be preferentially melted. However, simple calculations involving the Ti budget and melt mode suggest that the presence of residual rutile during partial melting is unlikely, as it would be entirely consumed after <0·5% partial melting (Coe, 2004). It is, therefore, interpreted that the relative depletion in Nb and Ta ($La/Nb_N > 1·3$; Fig. 4b) is a characteristic source feature of all Group II kimberlites analysed in this study. Furthermore, the presence of negative Nb and Ta anomalies in Karoo basalts (Marsh *et al.*, 1997), argued by some workers to represent subcontinental lithospheric melts (e.g. Hawkesworth *et al.*, 1984), as well as in some Kaapvaal craton xenoliths and their constituent minerals (van Achterbergh *et al.*, 2001; Grégoire *et al.*, 2003), suggests that this may be an important characteristic of the sub-Gondwana lithosphere.

Close-to-primary kimberlite magmas are, therefore, argued to have been unaffected by residual phlogopite or any titanate phases. Following the preferred models of le Roex *et al.* (2003) and Harris *et al.* (2004) for Group I and Coe (2004) for Group II close-to-primary kimberlite magmas, depletion in Rb, K, Ti and, to a lesser extent, Sr, Hf and Nb–Ta (Group II kimberlites) are characteristics inherited directly from their source regions.

Timing of source enrichment

Nd isotope signatures of on- and off-craton Group I kimberlites are depleted relative to present-day Bulk Earth; minimum Nd model ages calculated with respect to CHUR and Depleted Mantle suggest that metasomatic enrichment of their source regions occurred relatively recently (0–700 Ma), possibly just prior to the Jurassic–Cretaceous emplacement of Group I kimberlites. The Group II kimberlite sources, however, are characterized by time-integrated $^{143}Nd/^{144}Nd$ ratios indicative of ancient LREE source enrichment (this study; Smith, 1983; Fraser *et al.*, 1985–1986; Coe, 2004). Calculated model ages suggest source enrichment at 600–900 Ma relative to CHUR, or 1000–1300 Ma relative to Depleted Mantle, but, most importantly, they indicate that the source regions of Group II kimberlites were metasomatically enriched considerably prior to those of Group I kimberlites. Similar geochemical compositions and Nd model ages for both on- and off-craton Group II kimberlite source regions suggest enrichment after the collision of the Proterozoic Namaqua–Natal belt and the Kaapvaal craton at ~1·2–1·0 Ga (Thomas *et al.*, 1994).

DISCUSSION

The expanded geochemical dataset for both Group I and Group I kimberlites provided by this study affords the opportunity to investigate the cause of similarities and differences more rigorously than has been possible in the past, to investigate geodynamic relationships, to compare the influence of on- and off-craton settings, and to evaluate the possible origin of the metasomatic fluids that have enriched their mantle source regions.

On-craton vs off-craton differences

The role of tectonic setting, in terms of on- or off-craton locations, in controlling kimberlite geochemistry is ambiguous. Group II kimberlites show little systematic difference in major and trace element or Nd–Sr isotope geochemistry between on- and off-craton varieties, suggesting that both Proterozoic and Archaean mantle sources have experienced similar evolutionary histories leading up to Group II kimberlite magmatism. Both on- and off-craton Group II kimberlites appear to derive from within the garnet stability field, although the presence of diamonds in the on-craton kimberlites suggests derivation from greater depths. In contrast, off-craton Group I kimberlites tend to fall towards the low SiO_2 and MgO, but high FeO*, TiO_2, CaO and CO_2 ends of the compositional fields of their on-craton counterparts (Fig. 2), suggesting possible derivation from more fertile mantle sources (Boyd & McCallister, 1976; Janney *et al.*, 2001; Boyd *et al.*, 2004). Alternatively, experimental

studies suggest that partial melting at lower pressures results in a decrease in SiO_2 and MgO, and increase in FeO, Al_2O_3, CaO and CO_2 (e.g. Herzberg, 1992; Dalton & Presnall, 1998*b*; Gudfinnsson & Presnall, 2003), which would be consistent with the absence of diamonds in off-craton Group I kimberlites (Clifford, 1966), although both varieties are still derived from within the garnet stability field, based on similarly fractionated HREE patterns (Fig. 5a). LREE/HREE ratios also suggest that off-craton Group I kimberlites are higher degree melts than on-craton varieties (Fig. 8), in disagreement with the experimental studies of Dalton & Presnall (1998*a*) and Herzberg (1992), which indicate that partial melts become progressively richer in SiO_2 and MgO as the degree of melting increases.

Alternatives to a garnet lherzolite source

Given that the source regions of Group II kimberlites appear to be more highly enriched in incompatible elements than those of Group I kimberlites, a more exotic source mineralogy, corresponding to the 'clinopyroxene and mica rich-vein' model of Foley (1992*b*) needs to be considered. Foley (1992*b*) has argued that the source of ultrapotassic rocks is free of olivine, because of the absence of olivine as a liquidus phase in various experimental studies (e.g. Foley, 1992*a*; Girnis *et al.*, 1995), and that the resulting magmas are hybrids of vein (e.g. cpx, phlog, apatite, spinel) and wall-rock components (e.g. ol, opx, cpx, garnet) with initial melting taking place within the vein. The presence of cross-cutting veins in mantle samples is well established (e.g. Erlank *et al.*, 1987); these may represent the channelways for metasomatic fluids that then cryptically or modally metasomatize the wall rock, or are the final product of extensive modal metasomatism.

Grégoire *et al.* (2002) have recently published REE abundances in phlogopite and clinopyroxene from phlogopite-rich mantle xenoliths from the Kimberley region, which allows evaluation of the Foley (1992*b*) model. Clinopyroxene associated with phlogopite in such xenoliths appears to have chondrite-normalized REE patterns that are slightly convex upward with respect to the middle REE, i.e. La and Ce are slightly depleted relative to Nd and Sm, whereas phlogopite is virtually devoid of REE. The bulk composition thus essentially reflects uniform dilution of the clinopyroxene concentrations by the amount of phlogopite present. If one assumes a vein source comprising 50% each of clinopyroxene and phlogopite, then very low degrees of melting (1%) will give REE patterns reasonably similar with respect to the HREE, but very distinct with respect to the LREE from those seen in Group II kimberlites (Fig. 10), with the latter having very much steeper LREE patterns ($La/Sm_N = 8 \pm 2$, Table 4, vs $La/Sm_N \sim 2$ in the vein melts). One per cent melting is probably low for melting within a metasomatic vein, and more realistic higher degrees of melting will only exacerbate the discrepancy.

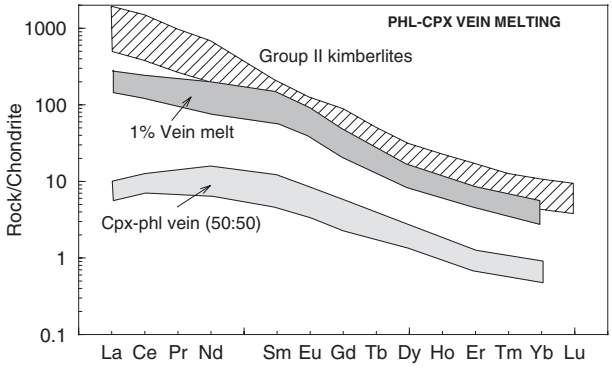

Fig. 10. Calculated chondrite-normalized REE patterns for a 1% partial melt of a clinopyroxene–phlogopite vein compared with average close-to-primary Group II kimberlite compositions. Vein composition calculated assuming 50% clinopyroxene and 50% phlogopite, using published REE abundances from clinopyroxene and phlogopite in clinopyroxene–phlogopite xenoliths from the Kimberley region (Grégoire *et al.*, 2002). Chondrite normalizing values are from Sun & McDonough (1989).

High Mg-number as well as Ni and Cr contents of close-to-primary Group II kimberlite magmas provide a further argument against a clinopyroxene–phlogopite vein source, in that they require equilibrium with refractory olivine at some stage during their petrogenesis. Similarly, Re–Os isotopes and Os population studies imply that Group II kimberlites are derived from melting of olivine-rich sources (Pearson *et al.*, 1995, 2003). These observations together suggest that if vein melting was involved, then considerable wall-rock interaction took place to give the kimberlites their refractory character.

Metasomatic veining is a variant of disseminated modal metasomatism (e.g. Menzies *et al.*, 1987), and the modelling technique used here is unable to discriminate the physical nature of metasomatic enrichment to this level of detail. Moreover, it is based on the modal residual mineralogy at the time of melt extraction; we therefore favour a model of melt generation from a modally metasomatized garnet lherzolite.

Role and origin of metasomatizing fluids

The geochemically enriched nature of the calculated Group I and Group II kimberlite source regions, coupled with the evidence for refractory compositions (high Mg-number and Ni; low Al_2O_3 and HREE), argues for metasomatic enrichment of a previously melt-depleted source region. Many peridotite xenoliths entrained by kimberlites show evidence for progressive metasomatism reflected in increasingly greater modal proportions of

phlogopite, ± K-richterite, but with lower proportions of garnet (Erlank *et al.*, 1987; Waters & Erlank, 1988). Textural and geochemical evidence indicates that phlogopite, clinopyroxene and Cr-spinel all grow at the expense of garnet (Erlank *et al.*, 1987; van Achterbergh *et al.*, 2001; Grégoire *et al.*, 2003; Simon *et al.*, 2003). These reactions are consistent with our earlier arguments that the distinct differences in REE ratios between Group I and Group II kimberlites, and the more Si, K and LILE-enriched character of the latter, are due to their sources having more clinopyroxene and phlogopite formed by metasomatism at the expense of garnet than those of Group I kimberlites. Group II kimberlites, are therefore interpreted to be derived from more highly metasomatized source regions than Group I kimberlites, and although there may be more phlogopite present in the source of the former, this phase is likely to be entirely consumed during partial melting (Ulmer & Sweeney, 2002).

It has been argued above that the source of both Group I and Group II kimberlites is the melt-depleted SCLM, enriched through percolation of metasomatic melts or fluids derived from sub-lithospheric sources. Hf isotope evidence from at least the MARID xenoliths in Group I kimberlites supports the involvement of the SCLM and asthenospheric mantle (Choukroun *et al.*, 2005). Differences in diagnostic trace element ratios and Sr and Nd isotope compositions of Group I and Group II kimberlites allow a comment on the likely origin of the metasomatic fluids responsible for the enrichment of their respective source regions. Group I kimberlites have unradiogenic Sr and radiogenic Nd isotope ratios, similar to ocean island basalts (OIB; Fig. 7), which led Smith (1983) to propose that their sources contain an asthenospheric component. More recently, le Roex *et al.* (2003) and Harris *et al.* (2004) have shown that certain diagnostic incompatible trace element ratios in Group I kimberlites correspond to those characteristic of OIB (e.g. Nb/U = 47 ± 10; Ce/Pb = 25 ± 5; Hofmann *et al.*, 1986). Figure 11 shows selected incompatible element ratios of Group I kimberlites from this study and the correlation with South Atlantic OIB compositions is clear, with Group I kimberlites having Ba/Nb <12, La/Nb <1·1, Ce/Pb >22 and Th/Nb <0·14. Given this strong correlation, and following le Roex *et al.* (2003) and Harris *et al.* (2004), we argue that the enrichment of Group I kimberlite SCLM source regions is a consequence of upward percolation of alkaline melts or fluids sourced from upwelling Mesozoic mantle plumes that impinged on the base of the lithosphere just prior to continental break-up. Nd model ages are consistent with this relatively recent enrichment. In a geodynamic context, the plumes are inferred to have provided both material, in the form of metasomatizing alkaline fluids or melts, and heat to initiate melting to give rise to Group I kimberlite magmatism. In this regard, le Roex (1986), le Roex *et al.* (2003) and Harris *et al.* (2004) have noted that the age of Cretaceous Group I kimberlite magmatism corresponds to the passage of southern Africa over the Shona and Bouvet mantle plumes, currently located in the South Atlantic. By analogy, and although not forming part of this study, source regions of older Group I southern African kimberlites (e.g. Premier, Kuruman cluster) would have been metasomatized by melts or fluids derived from sub-lithospheric upwellings beneath the craton during the Proterozoic.

Group II kimberlites have an isotope signature that requires ancient enrichment of their source regions, and subsequent isolation from the convecting mantle to allow development of their more extreme isotopic compositions that are unlike OIB (Fig. 7). In contrast to Group I kimberlites, diagnostic elemental ratios of Group II kimberlites are clearly very distinct from those characteristic of OIB (Fig. 11), largely as a result of their relative depletion in Nb and Ta, and enrichment in Pb. Group II kimberlites also have lower absolute TiO_2 contents with larger negative Ti anomalies than Group I kimberlites. Depletion in Nb and other HFSE is a classic signature of calc-alkaline magmas in subduction zones (e.g. Elliott *et al.*, 1997; Woodhead *et al.*, 1998), and it is evident from Fig. 11 that the fields for Group II kimberlites strongly overlap with those for calc-alkaline magmas. Fluids derived from subduction zones are characterized by raised Ba/Th ratios, whereas melts derived from the down-going sediment pile tend to have raised Th/Nb ratios (e.g. Elliott *et al.*, 1997; Woodhead *et al.*, 1998). Group II kimberlites trend towards high Ba/Th and Th/Nb ratios, suggesting that both subduction zone fluids and sediment melt were involved in the metasomatic overprint of their lithospheric mantle source regions. This is consistent with the model of Helmstaedt & Gurney (1984), who suggested that the sources of kimberlites were metasomatized by volatiles derived from subducted slabs.

Minimum Nd model ages and the similar geochemical characteristics of on- and off-craton Group II kimberlites suggest that metasomatic enrichment occurred after welding of the Proterozoic mantle underlying the Namaqua–Natal belt to the Archaean Kaapvaal craton. As no differences have been recognized between the isotopic and trace element signatures of on- and off-craton kimberlites, both Archaean and Proterozoic kimberlite source regions appear to have been enriched by the same metasomatic event. If multiple subduction and accretion events occurred during the 1·2–1·0 Ga formation and metamorphism of the Namaqua–Natal belt (Thomas *et al.*, 1994), similar to that imaged by the Lithoprobe study in Canada (e.g. Cook *et al.*, 1999), then upward percolating melts or fluids derived from the down-going slabs would have affected both overlying Proterozoic and Archaean mantle. Metasomatism by

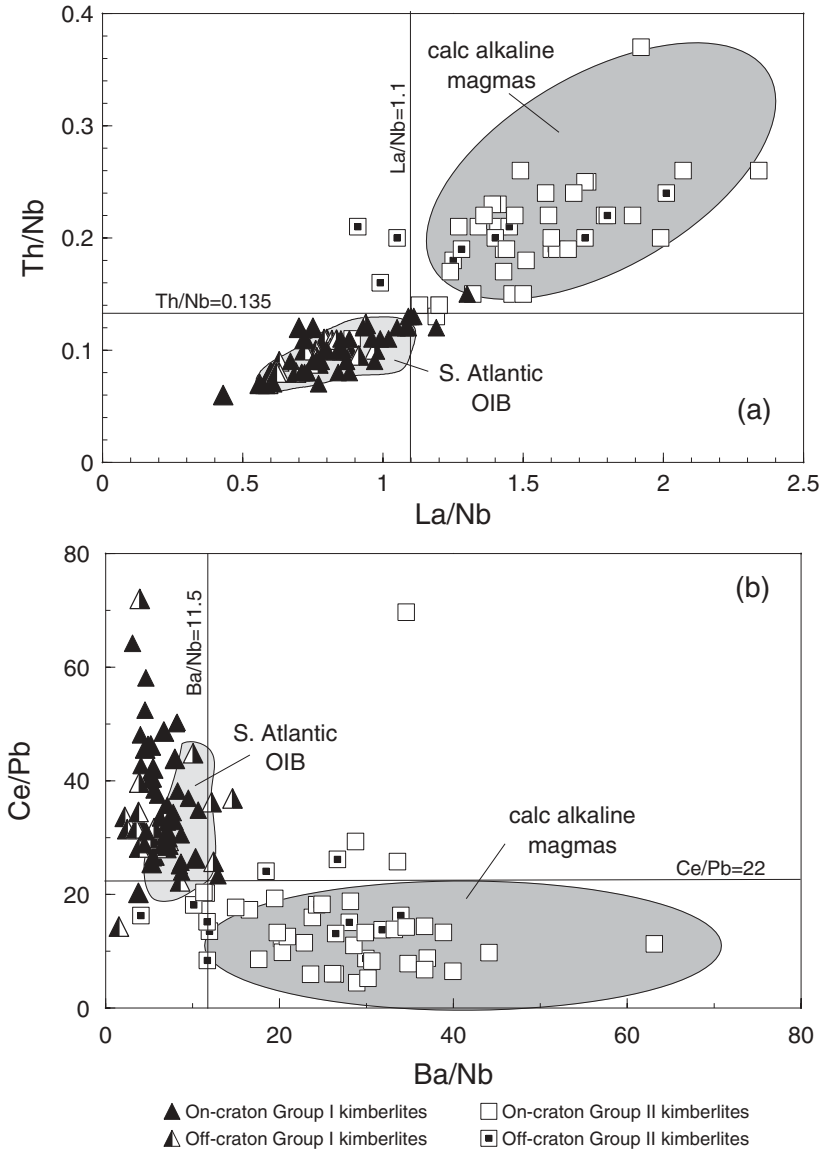

Fig. 11. Variation of (a) Th/Nb vs La/Nb and (b) Ce/Pb vs Ba/Nb for on- and off-craton Group I and Group II kimberlites. Dividing lines for Th/Nb, La/Nb, Ce/Pb and Ba/Nb provide distinction between kimberlite groups. Field of South Atlantic ocean island basalts (compilation from PetDB; www.petdb.ldeo.columbia.edu) and schematic field for calc-alkaline magmas (compilation from PetDB) are shown for comparison. Data from Kimberley (le Roex *et al.*, 2003), Uintjiesberg (Harris *et al.*, 2004), Swartruggens and Star (Coe, 2004) are included.

subduction zone fluids associated with the Pan-African event in southern Africa may also have contributed to the enrichment of on- and off-craton Group II kimberlite mantle source regions.

Independent support for this source region characteristic is found in the compositions of clinopyroxene in mantle xenoliths from both the Kaapvaal craton (e.g. Grégoire *et al.*, 2003), and the Namaqua–Natal belt (A. P. le Roex & C. Class, unpublished data, 2005). In both tectonic settings, clinopyroxenes with two distinctly different geochemical signatures can be identified, both showing evidence for metasomatic enrichment, but one having strong depletion in Nb and Ta and greater LREE enrichment.

McKenzie & O'Nions (1983) have argued that the sources of mantle plumes may be delaminated SCLM and thus, in theory, such plumes could be the source of metasomatic fluids with the Group II kimberlite geochemical signature. However, this is deemed unlikely as no OIB within the South Atlantic or Southern Ocean shows depletion in Nb or isotopic signatures similar to Group II kimberlites (le Roex & Erlank, 1982; le Roex, 1985; Hart, 1988; le Roex *et al.*, 1990). Although Tristan, Gough and Discovery OIB have high Ba/Nb ratios

similar to Group II kimberlites, this is a feature of high Ba in EM-1 OIB, thought to reflect a subducted sediment component in the mantle plume source, rather than depletion in Nb (le Roex, 1985; Sun & McDonough, 1989; Weaver, 1991). The palaeo-tracks of these particular OIB plumes also suggest that they are unlikely to have influenced South African kimberlite SCLM source regions (Hartnady & le Roex, 1985; le Roex, 1986; O'Connor & le Roex, 1992).

It is noteworthy that the 180 Ma Karoo continental flood basalts show similar depletion in Nb, Ta and Ti, with strongly enriched isotope signatures (Duncan *et al.*, 1984; Hawkesworth *et al.*, 1984), suggesting that they may have been derived from a common source region located within the sub-Gondwana continental lithosphere. After the massive outpouring of the Karoo continental flood basalts at 180 Ma (Marsh *et al.*, 1997), and the eruption of Group II kimberlites from 200 to 110 Ma (e.g. Skinner, 1989; Gurney *et al.*, 2005), the more highly metasomatized source appears to have been largely exhausted. Consequently, the younger (~110–70 Ma; Smith *et al.*, 1985*a*, 1994) on- and off-craton Group I kimberlites analysed in this study were derived from the more recently (Mesozoic) enriched lithospheric mantle carrying a plume signature. The off-craton Group I East Griqualand kimberlites (Abbotsford East and Zeekoegat) erupted at ~150 Ma (Davis, 1977; Smith *et al.*, 1985*a*), prior to many of the Group II kimberlites, were derived from a mantle source region apparently unaffected by subduction zone metasomatism, but enriched by melts or fluids that have been associated with the Bouvet mantle plume, inferred to have underlain East Griqualand at that time (le Roex, 1986). Although the geochemistry of Group II kimberlites shows no evidence for a plume component, it is possible that the Mesozoic mantle plumes lying beneath South Africa at the time of Gondwana break-up provided the heat source for partial melting within the overlying metasomatized lithospheric mantle that led to Group II kimberlite magmatism.

CONCLUSIONS

Detailed bulk-rock major and trace element and Nd–Sr isotope data of over 20 Group I and Group II kimberlites emplaced on and off the Kaapvaal craton allow recognition of clear similarities and differences in their geochemistry, and allow constraints to be placed on their genesis and the evolution of their mantle source regions.

(1) Group I kimberlites tend to have higher TiO_2, CaO and CO_2, but lower SiO_2 and K_2O, compared with Group II kimberlites, whereas Group II kimberlites have slightly higher Ni, and substantially higher Ba, Rb and Pb and lower Nb and Ta concentrations. Diagnostic trace element ratios of Group I kimberlites that distinguish them from Group II kimberlites include Ba/Nb <12, La/Nb <1·1, Ce/Pb >22 and Th/Nb <0·14. These differences are interpreted to reflect differences inherited from their respective source regions.

(2) Marginally lower SiO_2 and MgO, but higher TiO_2, CaO and CO_2, in off-craton Group I kimberlites compared with their on-craton counterparts suggest derivation of the former from slightly less depleted source regions, or at slightly lower pressures, than on-craton kimberlites. The lower La/Sm, La/Yb and Gd/Yb of off-craton Group I kimberlites also are consistent with derivation by slightly higher degrees of melting than on-craton kimberlites. No significant differences are observed between on- and off-craton Group II kimberlites.

(3) Semi-quantitative modelling indicates that the high Mg-number (0·82–0·89) and Ni (600–1400 ppm) contents coupled with strong enrichment in incompatible elements of both Group I and Group II close-to-primary kimberlites requires derivation from a refractory source that has subsequently been metasomatically enriched. Calculated source compositions are not unlike those observed in garnet lherzolites from the Kaapvaal craton, with La = 4–37 × chondrite and Yb = 0·9–3·6 × chondrite.

(4) Contrasting REE ratios between Group I and Group II kimberlites (higher La/Sm and La/Yb, and lower Gd/Yb in Group II kimberlites) suggest that the source regions of Group II kimberlites have a greater modal proportion of clinopyroxene but less garnet, consistent with being more highly metasomatized than the Group I kimberlite source regions.

(5) The requirement for a refractory source protolith that was subsequently metasomatically enriched prior to melting is taken to imply that the source region of both Group I and Group II kimberlites is located within the SCLM. Characteristic trace element and Nd–Sr isotope ratios indicate that source regions of on- and off-craton Group I kimberlites have been enriched by OIB-like fluids or melts associated with the passage of Mesozoic mantle plume(s) beneath the SCLM. Diagnostic Nd–Sr isotope and trace element ratios of Group II kimberlites are unlike those of Group I kimberlites or OIB, but show more affinity to calc-alkaline magmas. We interpret this to suggest ancient metasomatic enrichment associated with the infiltration of subduction zone derived fluids or melts, which affected both the Archaean and Proterozoic lithospheric source regions of Group II kimberlites. Mesozoic mantle plumes may have subsequently provided the heat source to initiate partial melting and Group II kimberlite generation at the time of continental break-up.

ACKNOWLEDGEMENTS

We are grateful to Dr Jock Robey for his help in the field, and Dr Craig Smith for making certain samples in the

De Beers sample store available to us. Finsch kimberlite analyses are from Noxolo Zwane's unpublished B.Sc.(Hons) project. Constructive reviews were received from Rick Carlson, Bill Griffin and Goonie Marsh. The National Research Foundation, De Beers Consolidated Mines (Ltd) and the University of Cape Town have all provided financial support for this research.

SUPPLEMENTARY DATA

Supplementary data for this paper are available at *Journal of Petrology* online.

REFERENCES

Allsopp, H. L. & Barrett, D. R. (1975). Rb–Sr age determinations on South African kimberlite pipes. *Physics and Chemistry of the Earth* **9**, 605–617.

Barrett, D. R. & Berg, G. W. (1975). Complementary petrographic and strontium-isotope ratio studies of South African kimberlite. *Physics and Chemistry of the Earth* **9**, 619–635.

Beard, A. D., Downes, H., Hegner, E., Sablukov, S. M., Vetrin, V. R. & Balogh, K. (1998). Mineralogy and geochemistry of Devonian ultramafic minor intrusions of the southern Kola Peninsula, Russia: implications for the petrogenesis of kimberlites and melilitites. *Contributions to Mineralogy and Petrology* **130**, 288–303.

Beard, A. D., Downes, H., Hegner, E. & Sablukov, S. M. (2000). Geochemistry and mineralogy of kimberlites from the Arkhangelsk Region, NW Russia: evidence for transitional kimberlite magma types. *Lithos* **51**, 47–73.

Beattie, P., Ford, C. & Russell, D. (1991). Partition coefficients for olivine–melt and orthopyroxene–melt systems. *Contributions to Mineralogy and Petrology* **109**, 212–224.

Becker, M. & le Roex, A. P. (in prep). Geochemistry and petrogenesis of South African isotopically transitional kimberlites located on and off the Kaapvaal Craton. *Lithos*.

Berg, G. W. & Allsopp, H. L. (1972). Low $^{87}Sr/^{86}Sr$ ratios in fresh South African kimberlites. *Earth and Planetary Science Letters* **16**, 27–30.

Birch, G. F. (1981). The karbonat-bombe; a precise, rapid and cheap instrument to determine calcium carbonate in sediments and rocks. *Transactions of the Geological Society of South Africa* **84**, 199–203.

Boyd, F. R. & McCallister, R. H. (1976). Densities of fertile and sterile garnet peridotites. *Geophysical Research Letters* **3**, 509–512.

Boyd, F. R. & Mertzman, S. A. (1987). Composition and structure of the Kaapvaal lithosphere, southern Africa. *Geochemical Society, Special Publications* **1**, 13–24.

Boyd, F. R. & Nixon, P. H. (1975). Origins of the ultramafic nodules from the kimberlites of northern Lesotho and the Monastery Mine, South Africa. *Physics and Chemistry of the Earth's Interior* **9**, 431–453.

Boyd, F. R., Pearson, D. G., Hoal, K. O., Hoal, B. G., Nixon, P. H., Kingston, M. J. & Mertzman, S. A. (2004). Garnet lherzolites from Louwrensia, Namibia: bulk composition and *P/T* relations. *Lithos* **77**, 573–592.

Canil, D. & Scarfe, C. M. (1990). Phase relations in peridotite + CO_2 systems to 12 GPa: implications for the origin of kimberlite and carbonate stability in the Earth's upper mantle. *Journal of Geophysical Research* **95**, 15805–15816.

Carlson, R. W., Boyd, F. R., Shirey, S. B., Janney, P. E., Grove, T. L., Bowring, S. A., Schmitz, M. D., Dann, J. C., Bell, D. R., Gurney, J. J., Richardson, S. H., Tredoux, M., Menzies, A. H., Pearson, D. G., Hart, R. J., Wilson, A. H. & Moser, D. (2000). Continental growth, preservation, and modification in southern Africa. *GSA Today* **10**, 1–7.

Chalapathi Rao, N. V., Gibson, S. A., Pyle, D. M. & Dickin, A. P. (2004). Petrogenesis of Proterozoic lamproites and kimberlites from the Cuddapah Basin and Dharwar Craton, southern India. *Journal of Petrology* **45**, 907–948.

Choukroun, M., O'Reilly, S. Y., Griffin, W. L., Pearson, N. J. & Dawson, J. B. (2005). Hf isotopes of MARID (mica–amphibole–rutile–ilmenite–diopside) rutile trace metasomatic processes in the lithospheric mantle. *Geology* **33**, 45–48.

Clark, T. C. (1994). An integrated geochemical and isotopic study of the Prieska Province kimberlites from the Republic of South Africa. M.Sc. thesis, University of the Witwatersrand.

Clement, C. R. (1982). A comparative geological study of some major kimberlite pipes in the Northern Cape and Orange Free State. Ph.D. thesis, University of Cape Town.

Clement, C. R. & Skinner, M. W. (1979). Textural genetic classification of kimberlites. *Transactions of the Geological Society of South Africa* **88**, 403–410.

Clement, C. R., Skinner, E. M. W. & Scott Smith, B. H. (1984). Kimberlite redefined. *Journal of Geology* **92**, 223–228.

Clifford, T. N. (1966). Tectono-metallogenic units and metallogenic provinces of Africa. *Earth and Planetary Science Letters* **1**, 241–434.

Coe, N. (2004). Petrogenesis of the Swartruggens and Star Group II kimberlite dyke swarms, South Africa. M.Sc. thesis, University of Cape Town, 146 pp.

Cook, F. A., van der Velden, A. R., Hall, K. W. & Roberts, B. J. (1999). Frozen subduction in Canada's Northwest Territories: Lithoprobe deep lithospheric reflection profiling of the western Canadian Shield. *Tectonics* **18**, 1–24.

Cornell, D. H., Hawkesworth, C. J., van Calsteren, P. & Scott, W. D. (1986). Sm–Nd study of Precambrian crustal development in the Prieska–Copperton region, Cape Province. *Transactions of the Geological Society of South Africa* **89**, 17–28.

Dalton, J. A. & Presnall, C. (1998*a*). The continuum of primary carbonatitic–kimberlitic melt compositions in equilibrium with lherzolite: data from the system CaO–MgO–Al_2O_3–SiO_2–CO_2 at 6 GPa. *Journal of Petrology* **39**, 1953–1964.

Dalton, J. A. & Presnall, D. C. (1998*b*). Carbonatitic melts along the solidus of model lherzolite in the system CaO–MgO–Al_2O_3–SiO_2–CO_2 from 3 to 7 GPa. *Contributions to Mineralogy and Petrology* **131**, 123–136.

Davis, G. L. (1977). The ages and uranium contents of zircons from kimberlites and associated rocks. *Carnegie Institution of Washington, Yearbook* **76**, 631–635.

de Wit, M. J., Roering, C., Hart, R. J., Armstrong, R. A., de Ronde, C. E. J., Green, R. W. E., Tredoux, M., Peberdy, E. & Hart, R. A. (1992). Formation of an Archean continent. *Nature* **357**, 553–562.

Duncan, A. R., Erlank, A. J. & Marsh, J. S. (1984). Regional geochemistry of the Karoo Igneous Province. *Special Publication of the Geological Society of South Africa* **13**, 355–388.

Edgar, A. D. & Charbonneau, H. E. (1993). Melting experiments on a SiO_2-poor, CaO-rich aphanitic kimberlite from 5–10 GPa and their bearing on sources of kimberlite magmas. *American Mineralogist* **78**, 132–142.

Eggler, D. H. & Wendlandt, R. F. (1979). Experimental studies on the relationship between kimberlite magmas and partial melting of peridotite. In: Boyd, F. R. & Meyer, H. O. A. (eds) *Kimberlites, Diatremes and Diamonds; their Geology, Petrology and Geochemistry*. Washington, DC: American Geophysical Union, pp. 330–338.

Elliott, T., Plank, T., Zindler, A., White, W. & Bourdon, B. (1997). Element transport from slab to volcanic front at the Mariana arc. *Journal of Geophysical Research* **102**, 14991–15019.

Erlank, A. J., Waters, F. G., Hawkesworth, C. J., Haggerty, S. E., Allsopp, H. L., Rickard, R. S. & Menzies, M. (1987). Evidence for mantle metasomatism in peridotite nodules from the Kimberley pipes, South Africa. In: Menzies, M. & Hawkesworth, C. J. (eds) *Mantle Metasomatism*. London: Academic Press: pp. 221–312.

Foley, S. (1992*a*). Petrological characterisation of the source components of potassic magmas: geochemical and experimental constraints. *Lithos* **28**, 187–204.

Foley, S. (1992*b*). Vein-plus-wall-rock melting mechanisms in the lithosphere and the origin of potassic magmas. *Lithos* **28**, 435–453.

Franz, L., Brey, G. P. & Okrusch, M. (1996). Steady state geotherm, thermal disturbances, and tectonic development of the lower lithosphere underneath the Gibeon Kimberlite Province, Namibia. *Contributions to Mineralogy and Petrology* **126**, 181–198.

Fraser, K. J. & Hawkesworth, C. J. (1992). The petrogenesis of group 2 ultrapotassic kimberlite from Finsch mine, South Africa. *Lithos* **28**, 327–345.

Fraser, K. J., Hawkesworth, C. J., Erlank, A. J., Mitchell, R. H. & Scott-Smith, B. H. (1985–1986). Sr, Nd and Pb isotope and minor element geochemistry of lamproites and kimberlites. *Earth and Planetary Science Letters* **76**, 57–70.

Girnis, A. V., Brey, G. P. & Ryabchikov, I. D. (1995). Origin of Group 1A kimberlites: fluid-saturated melting experiments at 45–55 kbar. *Earth and Planetary Science Letters* **134**, 283–296.

Grégoire, M., Bell, D. R. & le Roex, A. P. (2002). Trace element geochemistry of glimmerite and MARID mantle xenoliths: their relationship to kimberlite and to phlogopite-bearing peridotite revisited. *Contributions to Mineralogy and Petrology* **142**, 603–625.

Grégoire, M., Bell, D. R. & le Roex, A. P. (2003). Garnet lherzolites from the Kaapvaal Craton (South Africa): trace element evidence for a metasomatic history. *Journal of Petrology* **44**, 629–657.

Griffin, W. L., Pearson, N. J., Belousova, E., Jackson, S. E., van Achterberg, E., O'Reilly, S. Y. & Shee, S. R. (2000). The Hf isotope composition of cratonic mantle: LAM-MC-ICP-MS analysis of zircon megacrysts in kimberlites. *Geochimica et Cosmochimica Acta* **64**, 133–147.

Gudfinnsson, G. H. & Presnall, D. C. (2003). Continuous gradations among primary kimberlitic, carbonatitic, melilititic, and komatiitic melts in equilibrium with garnet lherzolite at 3–8 GPa. In: Mitchell, R. & Scott-Smith, B. (eds) *VIIIth International Kimberlite Conference, Victoria, BC, Canada, Extended Abstracts*.

Gurney, J. J., Helmstaedt, H. H., le Roex, A. P., Richardson, S. H. & Westerlund, K. J. (2005). Diamonds: crustal distribution and formation processes in time and space integrated into an advanced deposit model. *Economic Geology* (in press).

Haggerty, S. E. (1987). Metasomatic mineral titanates in upper mantle xenoliths. In: Nixon, P. H. (ed.) *Mantle Xenoliths*. New York: John Wiley, pp. 671–690.

Harris, M., le Roex, A. & Class, C. (2004). Geochemistry of the Uintjiesberg kimberlite, South Africa: petrogenesis of an off-craton, group I, kimberlite. *Lithos* **74**, 149–165.

Hart, S. R. (1977). The geochemistry and evolution of early Precambrian mantle. *Contributions to Mineralogy and Petrology* **61**, 109–128.

Hart, S. R. (1988). Heterogeneous mantle domains: signatures, genesis and mixing chronologies. *Earth and Planetary Science Letters* **90**, 273–296.

Hartnady, C. J. H. & le Roex, A. P. (1985). Southern Ocean hotspot tracks and the Cenozoic absolute motion of the African, Antarctic and South American plates. *Earth and Planetary Science Letters* **75**, 245–257.

Hawkesworth, C. J., Marsh, J. S., Duncan, A. R., Erlank, A. J. & Norry, M. J. (1984). The role of continental lithosphere in the generation of the Karoo volcanic rocks: evidence from combined Nd- and Sr-isotope studies. *Special Publication of the Geological Society of South Africa* **13**, 341–354.

Helmstaedt, H. & Gurney, J. J. (1984). Kimberlites of Southern Africa—are they related to subduction processes? In: Kornprobst, J. (ed.) *Kimberlites and Related Rocks: Kimberlites 1*. Amsterdam: Elsevier, pp. 424–435.

Herzberg, C. (1992). Depth and degree of melting of komatiites. *Journal of Geophysical Research* **97**, 4521–4540.

Herzberg, C. & O'Hara, M. J. (2002). Plume-associated ultramafic magmas of Phanerozoic age. *Journal of Petrology* **43**, 1857–1883.

Hofmann, A. W., Jochum, K. P., Seufert, M. & White, W. M. (1986). Nb and Pb in oceanic basalts: new constraints on mantle evolution. *Earth and Planetary Science Letters* **79**, 33–45.

Janney, P. E., Carlson, R. W., Shirey, S. B., Bell, D. R. & le Roex, A. P. (2001). Re–Os age and thermal structure of off-craton lithospheric mantle in western South Africa. *EOS Transactions, American Geophysical Union* **82**, 20.

le Roex, A. P. (1985). Geochemistry, mineralogy and magmatic evolution of the basaltic and trachytic lavas from Gough Island, South Atlantic. *Journal of Petrology* **26**, 149–186.

le Roex, A. P. (1986). Geochemical correlation between southern African kimberlites and South Atlantic hotspots. *Nature* **324**, 243–245.

le Roex, A. P. & Erlank, A. J. (1982). Quantitative evaluation of fractional crystallization in Bouvet Island lavas. *Journal of Volcanology and Geothermal Research* **13**, 309–338.

le Roex, A. P., Erlank, A. J. & Needham, H. D. (1981). Geochemical and mineralogical evidence for the occurrence of at least three distinct magma types in the 'Famous' region. *Contributions to Mineralogy and Petrology* **77**, 24–37.

le Roex, A. P., Cliff, R. A. & Adair, B. J. I. (1990). Tristan da Cunha, South Atlantic: geochemistry and petrogenesis of a basanite–phonolite lava series. *Journal of Petrology* **31**, 779–812.

le Roex, A. P., Späth, A. & Zartman, R. E. (2001). Lithospheric thickness beneath the southern Kenya Rift: implications from basalt geochemistry. *Contributions to Mineralogy and Petrology* **142**, 86–106.

le Roex, A. P., Bell, D. R. & Davis, P. (2003). Petrogenesis of group I kimberlites from Kimberley, South Africa: evidence from bulk-rock geochemistry. *Journal of Petrology* **44**, 2261–2286.

le Roux, P. J., le Roex, A. P., Schilling, J.-G., Shimizu, N., Perkins, W. W. & Pearce, N. J. G. (2002). Mantle heterogeneity beneath the southern Mid-Atlantic Ridge: trace element evidence for contamination of ambient asthenospheric mantle. *Earth and Planetary Science Letters* **203**, 479–498.

Maaloe, S. & Aoki, K.-i. (1977). The major element composition of the upper mantle estimated from the composition of lherzolites. *Contributions to Mineralogy and Petrology* **63**, 161–173.

Marsh, J. S., Hooper, P. R., Rehacek, J., Duncan, R. A. & Duncan, A. R. (1997). *Stratigraphy and Age of Karoo Basalts of Lesotho and Implications for Correlations within the Karoo Igneous Province*. Washington, DC: American Geophysical Union.

Mathias, M., Siebert, J. C. & Rickwood, P. C. (1970). Some aspects of the mineralogy and petrology of ultramafic xenoliths in kimberlite. *Contributions to Mineralogy and Petrology* **26**, 75–123.

McKenzie, D. & O'Nions, R. K. (1983). Mantle reservoirs and ocean island basalts. *Nature* **301**, 229–231.

Menzies, M., Rogers, N., Tindle, A. & Hawkesworth, C. J. (1987). Metasomatic and enrichment processes in lithospheric peridotites,

and effect of asthenosphere–lithosphere interaction. In: Menzies, M. & Hawkesworth, C. J. (eds) *Mantle Metasomatism*. London: Academic Press, pp. 313–361.

Mitchell, R. (1995). *Kimberlites, Orangites and Related Rocks*. New York: Plenum.

Mitchell, R. H. (2004). Experimental studies at 5–12 GPa of the Ondermatjie hypabyssal kimberlite. *Lithos* **76**, 551–564.

Nixon, P. H., Boyd, F. R. & Boctor, N. Z. (1983). East Griqualand kimberlites. *Transactions of the Geological Society of South Africa* **86**, 221–236.

Nowell, G. M., Pearson, D. G., Kempton, P. D., Noble, S. R. & Smith, C. B. (1999). Origins of kimberlites: a hafnium perspective. In: Gurney, J. J., Gurney, J. L., Pascoe, M. D. & Richardson, S. H. (eds) *Proceedings of the VIIth International Kimberlite Conference*. Cape Town: Red Roof Design, pp. 616–624.

Nowell, G. M., Pearson, D. G., Bell, D. R., Carlson, R. W., Smith, C. B., Kempton, P. D. & Noble, S. R. (2004). Hf isotope systematics of kimberlites and their megacrysts: new constraints on their source regions. *Journal of Petrology* **45**, 1583–1612.

O'Connor, J. M. & le Roex, A. P. (1992). South Atlantic hot spot-plume systems: 1. Distribution of volcanism in time and space. *Earth and Planetary Science Letters* **113**, 343–364.

O'Nions, R. K. & Pankhurst, R. J. (1974). Petrogenetic significance of isotope and trace element variations in volcanic rocks from the Mid-Atlantic. *Journal of Petrology* **15**, 603–634.

O'Nions, R. K., Hamilton, P. J. & Evensen, N. M. (1977). Variations in $^{143}Nd/^{144}Nd$ and $^{87}Sr/^{86}Sr$ ratios in oceanic basalts. *Earth and Planetary Science Letters* **34**, 13–22.

Pearson, D. G. & Nowell, G. M. (2002). The continental lithospheric mantle: characteristics and significance as a mantle reservoir. *Philosophical Transactions of the Royal Society of London, Series A* **360**, 2383–2410.

Pearson, D. G., Rogers, N. W., Irving, A. J., Smith, C. B. & Hawkesworth, C. J. (1995). Source regions of kimberlites and lamproites: constraints from Re–Os isotopes. In: *VIth International Kimberlite Conference, Extended Abstracts*. Novosibirsk: Russian Academy of Sciences, United Institute of Geology, Geophysics and Mineralogy, pp. 430–432.

Pearson, D. G., Nowell, G. M., Dowall, D. P., Kjarsgaard, B. A., Kopylova, M. G. & Armstrong, J. A. (2003). The relative roles of lithosphere and convecting mantle in kimberlites from the Slave Province, NWT: constraints from Re–Os isotopes and olivine population studies. *VIIIth International Kimberlite Conference, Extended Abstracts*.

Phillips, D., Harris, J. W. & Viljoen, K. S. (2004). Mineral chemistry and thermobarometry of inclusions for De Beers pool diamonds, Kimberley, South Africa. *Lithos* **77**, 155–179.

Pretorious, D. A. (1974). The structural boundary between the Kaapvaal craton and the Sanama crustal provinces. In: *Information Circular of Economic Geology Research Unit*. Johannesburg: University of the Witwatersrand, 26 pp.

Price, S. E., Russell, J. K. & Kopylova, M. G. (2000). Primitive magma from the Jericho Pipe, N.W.T., Canada: constraints on primary kimberlite melt chemistry. *Journal of Petrology* **41**, 789–808.

Robey, J. (1981). Kimberlites in the Central Cape Province, R.S.A. Ph.D. thesis, University of Cape Town.

Rogers, N. W., Hawkesworth, C. J. & Palacz, Z. A. (1992). Phlogopite in the generation of olivine-melilitites from Namaqualand, South Africa, and its implications for element fractionation processes in the upper mantle. *Lithos* **28**, 347–365.

Schmidt, K. H., Bottazzi, P., Vannucci, R. & Mengel, K. (1999). Trace element partitioning between phlogopite, clinopyroxene and leucite lamproite melt. *Earth and Planetary Science Letters* **168**, 287–300.

Schmitz, M. D., Bowring, S. A., de Wit, M. J. & Gartz, V. (2004). Subduction and terrane collision stabilize the western Kaapvaal craton tectosphere 2·9 billion years ago. *Earth and Planetary Science Letters* **222**, 363–376.

Shee, S. R. (1985). The petrogenesis of the Wesselton Mine Kimberlite, Kimberley, Cape Province, R.S.A. Ph.D. thesis, University of Cape Town.

Simon, N. S. C., Irvine, G. J., Davies, G. R., Pearson, D. G. & Carlson, R. W. (2003). The origin of garnet and clinopyroxene in 'depleted' Kaapvaal peridotites. *Lithos* **71**, 289–322.

Skinner, E. M. W. (1989). Contrasting Group I and Group II kimberlite petrology: towards a genetic model for kimberlites. In: Ross, J., Jacques, A. L., Ferguson, J., Green, D. H., O'Reilly, S. Y., Danchin, R. V. & Janse, A. J. A. (eds) *IVth International Kimberlite Conference*. Perth: Geological Society of Australia, pp. 528–544.

Skinner, E. M. W., Smith, C. B., Viljoen, K. S. & Clark, T. C. (1992). The petrography, tectonic setting and emplacement ages of kimberlites in the south western border region of the Kaapvaal Craton, Prieska area, South Africa. In: Meyer, H. O. A. & Leonardos, O. H. (eds) *Kimberlites, Related Rocks and Mantle Xenoliths*. Brasilia: CPRM, pp. 80–97.

Smith, C. B. (1983). Pb, Sr and Nd isotopic evidence for sources of southern African Cretaceous kimberlites. *Nature* **304**, 51–54.

Smith, C. B., Allsopp, H. L., Kramers, J. D., Hutchinson, G. & Roddick, J. C. (1985*a*). Emplacement ages of Jurassic–Cretaceous South African kimberlites by the Rb–Sr method on phlogopite and whole-rock samples. *Transactions of the Geological Society of South Africa* **88**, 249–266.

Smith, C. B., Gurney, J. J., Skinner, E. M. W., Clement, C. R. & Ebrahim, N. (1985*b*). Geochemical character of the southern African kimberlites: a new approach based on isotopic constraints. *Transactions of the Geological Society of South Africa* **88**, 267–280.

Smith, C. B., Clark, T. C., Barton, E. S. & Bristow, J. W. (1994). Emplacement ages of kimberlite occurrences in the Prieska region, southwest border of the Kaapvaal Craton, South Africa. *Chemical Geology* **113**, 149–169.

Späth, A., le Roex, A. P. & Opiyo-Akech, N. (2001). Plume–lithosphere interaction and the origin of continental rift-related alkaline volcanism—the Chyulu Hills Volcanic Province, southern Kenya. *Journal of Petrology* **42**, 765–787.

Sun, S.-s. & McDonough, W. F. (1989). Chemical and isotopic systematics of oceanic basalts: implications for mantle composition and processes. In: Saunders, A. D. & Norry, M. J. (eds) *Magmatism in the Ocean Basins*. *Geological Society, London, Special Publications* **42**, 313–345.

Tainton, K. M. (1992). The petrogenesis of group-2 kimberlites and lamproites from the Northern Cape Province, South Africa. Ph.D. thesis, Cambridge.

Tainton, K. M. & McKenzie, D. (1994). The generation of kimberlites, lamproites, and their source rocks. *Journal of Petrology* **35**, 787–817.

Thomas, R. J., Agenbacht, A. L. D., Cornell, D. H. & Moore, J. M. (1994). The Kibaren of southern Africa: tectonic evolution and metallogeny. *Ore Geology Reviews* **9**, 131–160.

Ulmer, P. & Sweeney, R. J. (2002). Generation and differentiation of group II kimberlites: constraints from a high-pressure experimental study to 10 GPa. *Geochimica et Cosmochimica Acta* **66**, 2139–2153.

van Achterbergh, E., Griffin, W. L. & Stiefenhofer, J. (2001). Metasomatism in mantle xenoliths from the Letlhakane kimberlites: estimation of element fluxes. *Contributions to Mineralogy and Petrology* **141**, 397–414.

Wagner, P. A. (1914). *The Diamond Fields of Southern Africa*. Johannesburg: Transvaal Leader.

Walker, R. J., Carlson, R. W., Shirey, S. B. & Boyd, F. R. (1989). Os, Sr, Nd, and Pb isotope systematics of southern African peridotite xenoliths; implications for the chemical evolution of subcontinental mantle. *Geochimica et Cosmochimica Acta* **53**, 1583–1595.

Wass, S. Y. & Rogers, N. W. (1980). Mantle metasomatism—precursor to continental alkaline volcanism. *Geochimica et Cosmochimica Acta* **44**, 1811–1823.

Waters, F. G. & Erlank, A. J. (1988). Assessment of the vertical extent and distribution of mantle metasomatism below Kimberley, South Africa. *Journal of Petrology*, 185–204.

Weaver, B. L. (1991). Trace element evidence for the origin of ocean-island basalts. *Geology* **19**, 123–126.

Wedepohl, K. H. & Muramatsu, Y. (1975). *The Chemical Composition of Kimberlites Compared with the Average Composition of Three Basaltic Magma Types*. Washington, DC: American Geophysical Union.

Williams, H. M., Turner, S. P., Pearce, J. A., Kelley, S. P. & Harris, N. B. W. (2004). Nature and source regions for post-collisional, potassic magmas in southern and northern Tibet from geochemical variation and inverse trace element modelling. *Journal of Petrology* **45**, 555–607.

Willis, J. P. (1999). *Instrumental Parameters and Data Quality for Routine Major and Trace Element Determinations by WDXRFS*. Cape Town: University of Cape Town.

Woodhead, J. D., Eggins, S. M. & Johnson, R. W. (1998). Magma genesis in the New Britain Island Arc: further insights into melting and mass transfer process. *Journal of Petrology* **39**, 1641–1668.

Yamashita, H., Arima, M. & Ohtani, E. (1995). High pressure melting experiments on group II kimberlite up to 8 GPa: implications for mantle metasomatism. In: *VIth International Kimberlite Conference, Extended Abstracts*. Novosibirsk: Russian Academy of Sciences, United Institute of Geology, Geophysics and Mineralogy, pp. 669–671.

Zindler, A. (1980). Geochemical processes in the Earth's mantle and the nature of crust–mantle interactions: evidence from studies of Nd and Sr isotope ratios in mantle derived igneous rocks and lherzolite nodules. Ph.D. thesis, MIT, Cambridge, MA.